

# Lawrence Berkeley National Laboratory

LBL Publications

## Title

Cooperative Brønsted-Lewis acid sites created by phosphotungstic acid encapsulated metal-organic frameworks for selective glucose conversion to 5-hydroxymethylfurfural

## Permalink

<https://escholarship.org/uc/item/80x495z8>

## Authors

Rahaman, Mohammad Shahinur

Tulaphol, Sarttrawut

Hossain, Anwar

et al.

## Publication Date

2022-02-01

## DOI

10.1016/j.fuel.2021.122459

## Copyright Information

This work is made available under the terms of a Creative Commons Attribution-NonCommercial License, available at <https://creativecommons.org/licenses/by-nc/4.0/>

Peer reviewed

1 **Cooperative Brønsted-Lewis acid sites created by phosphotungstic acid encapsulated metal-organic**  
2 **frameworks for selective glucose conversion to 5-hydroxymethylfurfural**

3

4 Mohammad Shahinur Rahaman<sup>1</sup>, Sarttrawut Tulaphol<sup>1,2</sup>, Md Anwar Hossain<sup>1</sup>, Jacek B. Jasinski<sup>3</sup>, Ning  
5 Sun<sup>4,5</sup>, Anthe George<sup>6,7</sup>, Blake Simmons<sup>4,7</sup>, Thana Maihom<sup>8</sup>, Mark Crocker<sup>9,10</sup>, and Noppadon  
6 Sathitsuksanoh<sup>1\*</sup>

7

8 <sup>1</sup>Department of Chemical Engineering, University of Louisville, Louisville, KY 40292, USA

9 <sup>2</sup>Sustainable Polymer & Innovative Composite Materials Research Group, Department of Chemistry, Faculty of  
10 Science, King Mongkut's University of Technology Thonburi, Bangkok, Thailand 10140

11 <sup>3</sup>Conn Center for Renewable Energy Research, University of Louisville, Louisville, KY 40292, USA

12 <sup>4</sup>Lawrence Berkeley National Laboratory, Berkeley, CA 94720, USA

13 <sup>5</sup>Advanced Biofuels and Bioproducts Process Demonstration Unit, Emeryville, CA 94608, USA

14 <sup>6</sup>Sandia National Laboratories, 7011 East Ave, Livermore, CA 94551, USA

15 <sup>7</sup>Joint BioEnergy Institute, Emeryville, CA 94608, USA

16 <sup>8</sup>Department of Chemistry, Faculty of Liberal Arts and Science, Kasetsart University, Kamphaeng Saen Campus,  
17 Nakhon Pathom 73140, Thailand

18 <sup>9</sup>Center for Applied Energy Research, University of Kentucky, 2540 Research Park Drive, Lexington, KY 40511, USA

19 <sup>10</sup>Department of Chemistry, University of Kentucky, Lexington, KY 40506, USA

20

21 \* Corresponding author: N.sathitsuksanoh@louisville.edu

22

23

24

## 25 **Abstract**

26 Production of 5-hydroxymethylfurfural (HMF) from biomass-derived glucose has great potential for  
27 synthesis of renewable fuels and chemicals. Selective glucose conversion to 5-hydroxymethylfurfural  
28 requires a balance between Lewis and Brønsted acids for the cascade of glucose isomerization followed  
29 by fructose dehydration. A dual Brønsted-Lewis acid, phosphotungstic acid encapsulated MIL-101(Al)-  
30 NH<sub>2</sub> metal-organic frameworks (MOFs) was developed to catalyze the glucose dehydration reaction. The  
31 encapsulated catalysts had a high HMF selectivity of 58% at 44% glucose conversion at 120°C in  
32 [C<sub>4</sub>C<sub>1</sub>im]Cl. Phosphotungstic acid was uniformly dispersed in the MOF pores, which provided both  
33 Brønsted and Lewis acid sites for this cascade reaction. The Brønsted acidic phosphotungstic acid-  
34 encapsulated MOF catalyst was stable and recyclable at least four times. These findings explain the  
35 effect of phosphotungstic acid location for maximizing the HMF selectivity and suggest a new approach  
36 for the design of bifunctional solid acid catalysts for selective HMF production from glucose. Moreover,  
37 the tunability of the acid properties of the encapsulated MOF catalysts provides opportunities for other  
38 biomass transformations.

39

40 **Keywords.** Metal-organic frameworks; phosphotungstic acid; encapsulation; glucose dehydration;  
41 hydroxymethylfurfural, cooperative

42

## 43 **1. Introduction**

44 Negative consequences of fuel and chemical production from petroleum, especially sizeable greenhouse  
45 gas emissions, price volatility [1], and non-renewability [2], have propelled the production of commodity  
46 chemicals from renewable plant biomass. Hydroxymethylfurfural (HMF) is a versatile platform chemical

47 derived from biomass with potential applications for fuels, chemicals, plastics, and pharmaceuticals [3-  
48 5]. The challenge of glucose dehydration to HMF is to obtain high HMF selectivity. Although the glucose  
49 dehydration reaction has been studied extensively, its mechanism is still being debated [6, 7].

50 In general, glucose dehydration to HMF can occur by two chemical pathways (**Scheme 1**), direct  
51 dehydration (path 1) and tandem isomerization-dehydration reactions (path 2). The direct dehydration  
52 of glucose to HMF by Brønsted acid catalysts is slow, and HMF selectivity is low because of side  
53 reactions such as cross-condensation with formation of undesired humins [8-11]. Tandem isomerization-  
54 dehydration reactions in one-pot afford opportunities to transform glucose to HMF selectively [12].  
55 Selective production of HMF from glucose requires cooperation between Lewis and Brønsted acid  
56 catalysts for glucose isomerization to fructose and subsequent fructose dehydration to HMF [8, 13-15].  
57 Lewis acid promotes the isomerization of glucose to fructose and then dehydration of fructose to HMF  
58 by Brønsted acid [16-18].

59 Swift et al. demonstrated this concept of tandem isomerization-dehydration reactions by  
60 incorporating a Lewis acid ( $\text{CrCl}_3$ ) with a Brønsted acid (HCl) catalyst, an approach that enhanced both  
61 catalytic activity for glucose dehydration and HMF selectivity [19]. Vieira et al. used the combination of  
62 Lewis acid  $\text{Nb}_2\text{O}_5$  and Brønsted acid HCl in a water/tetrahydrofuran (THF) biphasic system. They found  
63 that the Brønsted acid HCl was necessary to improve HMF selectivity from 7.6% to 51% and glucose  
64 conversion from 49% to 93%, compared with  $\text{Nb}_2\text{O}_5$  alone [18]. Nikolla et al. used the combination of Sn-  
65 containing  $\beta$ -zeolite and HCl in  $\text{H}_2\text{O}$ /THF biphasic system to reach 72% HMF selectivity at 79% glucose  
66 conversion [20]. However, all these studies were conducted with homogeneous Brønsted acid catalysts  
67 that complicate product purification [21] and catalyst recycling. Therefore, it would be most useful to  
68 have solid catalysts that possess both Brønsted and Lewis acid active sites for selective glucose

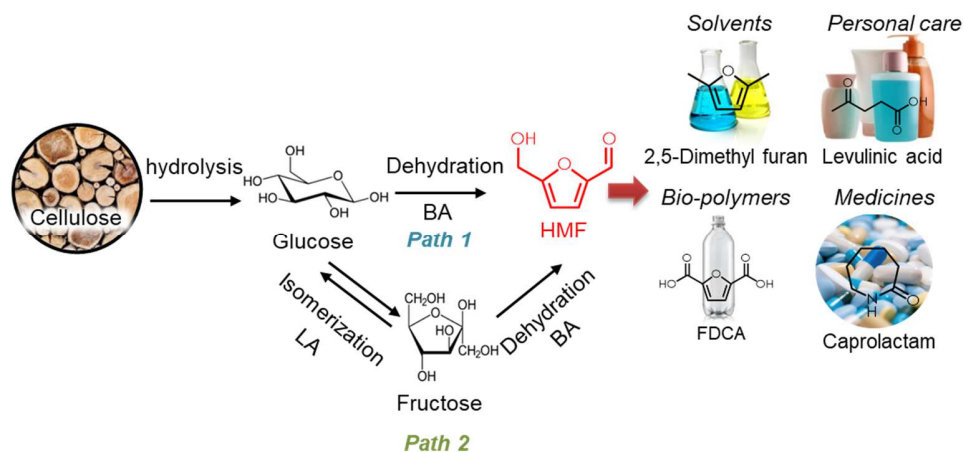
69 conversion to HMF. In answer to this need, this report describes metal-organic frameworks that have  
70 both Brønsted and Lewis acid sites for selective glucose conversion to HMF.

71 Metal-organic frameworks (MOFs) are porous crystalline materials that consist of metal ions or  
72 clusters coordinated with organic linkers to form highly uniform solid networks [22-27]. The coordinated  
73 unsaturated metal sites (cus) endow MOFs with Lewis acidity [28, 29]. Lewis acid sites of MOFs have  
74 been used to catalyze various reactions, such as aldol condensation [30], deacetalization-Knoevenagel  
75 condensation [31, 32], Meinwald rearrangement [33], and CO oxidation [34]. The porosity of MOFs  
76 enables incorporation of large Brønsted acidic molecules to create bifunctional acid catalysts for various  
77 acid-catalyzed organic reactions [22, 23, 35-38].

78 Polyoxometalates (POMs) are versatile catalysts because of their many active sites [39, 40]. The  
79 Keggin family of POMs ( $[XM_{12}O_{40}]^n$  anions (X = Si and P, M = Mo and W) with protons as the only  
80 counterions are heteropolyacids; examples include phosphotungstic acid, silicotungstic acid,  
81 silicomolybdic acid, and phosphomolybdic acid. These heteropolyacids have high acid strength and they  
82 are less corrosive compared with ordinary mineral acids (HBr, H<sub>2</sub>SO<sub>4</sub>, HNO<sub>3</sub>, and HCl) [41, 42]. Although  
83 these properties make heteropolyacids attractive in acid-catalyzed reactions [43-47], they are soluble in  
84 water and many organic solvents. Thus, they are difficult to recycle, and their presence complicates  
85 purification of soluble products.

86  
87 Trapping heteropolyacids in MOF pores generates bifunctional catalysts with both Lewis and  
88 Brønsted acids, which are important for selective glucose conversion to HMF [15, 48]. Indeed, as  
89 reported in **Table S2**, the Keggin-type heteropolyacids have been encapsulated successfully in the pores  
90 of MOFs [49-52]. For example, phosphotungstic acid (PTA)-encapsulated MIL-101(Cr) was used for  
91 various catalytic reactions such as the esterification of *n*-butanol with acetic acid [53], dehydration of

92 methanol [53], oxidative desulfurization of dibenzothiophene[54], carbohydrate dehydration to 5-  
 93 hydroxymethylfurfural [52], and oxidation of the alkenes [55]. Zhang et al. synthesized PTA◊MIL-101(Cr)  
 94 by encapsulating PTA in MIL-101(Cr) for sugar dehydration [52]. Fructose dehydration by PTA◊MIL-  
 95 101(Cr) was selective for HMF (77% HMF selectivity at 82% fructose conversion). However, PTA◊MIL-  
 96 101(Cr) was not selective for HMF in glucose dehydration (10% HMF selectivity at 21% glucose  
 97 conversion). Moreover, the use of fructose as a feedstock is not cost-effective because glucose is less  
 98 expensive than fructose [56]. In addition, the chromium in PTA◊MIL-101(Cr) catalysts is harmful to  
 99 humans, animals, and the environment [57]. Therefore, there is a need to develop heterogeneous  
 100 chromium-free acid catalytic systems that possess both Brønsted and Lewis acid sites to regulate the  
 101 HMF selectivity in glucose dehydration.



102

103 **Scheme 1.** Reaction network of HMF production (BA = Brønsted acid, LA = Lewis acid)

104 Here, this work describes encapsulation of phosphotungstic acid in the pores of MIL-101(Al)-NH<sub>2</sub>  
 105 to form PTA◊MIL-101(Al)-NH<sub>2</sub>. The effect of PTA encapsulation on catalytic performance in glucose  
 106 dehydration with [C<sub>4</sub>C<sub>1</sub>im]Cl as solvent was evaluated. The [C<sub>4</sub>C<sub>1</sub>im]Cl was selected as the reaction  
 107 solvent because our previous studies established that the alkyl imidazolium chloride ionic liquids, such  
 108 as [C<sub>2</sub>C<sub>1</sub>im]Cl and [C<sub>4</sub>C<sub>1</sub>im]Cl, can dissolve cellulose and enable hydrolysis of cellulose to sugars [58-60].

109 The MIL-101(Al)-NH<sub>2</sub> was selected because it is chemically and thermally stable [32]. Moreover,  
110 Brønsted acidic PTA was used as the heteropolyacid because it has a high acid strength compared with  
111 other heteropolyacids[61]. The encapsulated PTA in MIL-101(Al)-NH<sub>2</sub> was uniformly dispersed and stable  
112 in NH<sub>2</sub>-MIL-101(Al) pores, and it provided Brønsted acid sites that rendered the catalyst selective for  
113 HMF production. These results reveal the unrecognized catalytic performance of the PTA@MIL-101(Al)-  
114 NH<sub>2</sub> catalysts for selective glucose dehydration.

115

## 116 **2. Materials and Methods**

### 117 **2.1 Materials**

118 The following chemicals were purchased and used as received: D-glucose, 1-butyl-3-methylimidazolium  
119 chloride ([C<sub>4</sub>C<sub>1</sub>im]Cl), 2-aminoterephthalic acid (2-ATA), aluminum chloride hexahydrate,  
120 phosphotungstic acid (PTA), and *N,N*-dimethylformamide (DMF), methanol, ethanol, *n*-propanol, 2-  
121 propanol, *n*-butanol, 2-butanol, *p*-dioxane, ethyl acetate (EA), *N,N*-dimethylformamide (DMF), *N,N*-  
122 dimethylacetamide (DMA), dimethyl sulfoxide (DMSO), and tetrahydrofuran (THF). **Table S1** summarizes  
123 the list of chemicals/reagents, their supplier, purity, and CAS number. All other chemicals, solvents, and  
124 gases were of the highest purity available from commercial sources.

125

126

## 127 **2.2 Synthesis of metal-organic frameworks**

### 128 **2.2.1 Synthesis of MIL-101(Al)-NH<sub>2</sub>**

129 MIL-101(Al)-NH<sub>2</sub> was synthesized by the solvothermal method with a slight modification [62]. Typically,  
130 a mixture of aluminum chloride hexahydrate (0.51 g, 2 mmol) and 2-aminoterephthalic acid (0.56 g, 3  
131 mmol) in DMF (30 mL) was kept in a Teflon-lined autoclave reactor without stirring at 130 °C for 72 h.  
132 Then the reactor was cooled to ambient temperature, and the solids were separated from the solution  
133 by centrifugation (6000 RPM, 5 min). The solids were washed with DMF under sonication for 10 min.  
134 Finally, the solid catalysts were washed three times with methanol at room temperature followed by  
135 washing with hot (70 °C) methanol for 5 h and dried overnight under vacuum at 80 °C.

136

### 137 **2.2.2 Synthesis of encapsulated PTA in MIL-101(Al)-NH<sub>2</sub> (PTA@MIL-101(Al)-NH<sub>2</sub>)**

138 PTA@MIL-101(Al)-NH<sub>2</sub> was synthesized by incorporating phosphotungstic acid (PTA) hydrated during the  
139 synthesis of MIL-101(Al)-NH<sub>2</sub>. In short, aluminum chloride hexahydrate (0.51 g, 2.1 mmol), 2-amino  
140 terephthalic acid (0.56 g, 3.1 mmol), and different amounts of PTA hydrate (0.1-2.0 g) in DMF (30 mL,  $\rho$   
141 = ~0.9 g/mL) were kept in a Teflon-lined autoclave reactor without stirring, and the mixture was heated  
142 at 130 °C for 72 h. After cooling to ambient temperature, the resulting solids were separated by  
143 centrifugation (6000 RPM, 5 min), washed with DMF, then washed with hot methanol (70°C), and finally  
144 washed with acetone, and dried under vacuum at 80 °C overnight.

145

## 146 **2.3 Catalyst characterization**

### 147 **2.3.1 Transmission electron microscopy and energy-dispersive X-ray spectroscopy analysis**

148 The microstructure and elemental distribution of the metal-organic frameworks (MOFs) were analyzed  
149 using transmission electron microscopy (TEM) in a Tecnai F20 (FEI company, OR, USA) microscope  
150 operating at 200 kV. TEM specimens were prepared by dispersing small amounts of catalysts onto Cu



151 grid-supported holey carbon films. For the analysis of the microstructure, scanning transmission  
152 electron microscopy (STEM) images were acquired with a high annular angle dark field (HAADF) detector  
153 (E.A. Fischione Instruments, Inc., PA, USA) and an electron probe of a 1 nm diameter. For the elemental  
154 distribution analysis, energy-dispersive X-ray spectroscopy (EDS) maps were collected using a TEAM EDS  
155 (EDAX, Inc., NJ, USA) spectrometer.

156

### 157 **2.3.2 N<sub>2</sub> adsorption-desorption**

158 The N<sub>2</sub> adsorption-desorption assay was conducted with a Micromeritics Tristar (Norcross, GA, USA)  
159 instrument. The function of TriStar was verified with reference materials (Micromeritics). Prior to the  
160 measurement, the samples were pretreated with a Micromeritics FlowPrep with sample degasser  
161 (Norcross, GA, USA) at 160 °C for 2 h. The surface area,  $S_{\text{BET}}$ , was determined from N<sub>2</sub> isotherms using  
162 the Brunauer–Emmett–Teller equation (BET) at -196.15 °C (77 K) [63, 64]. The BET model assumes  
163 multilayer gas adsorption on the adsorbent's surface and obtains the sample surface area value by  
164 determining the monolayer volume of adsorbed gas from the isotherm data [65, 66]. BET surface area  
165 was calculated at relative pressures between 0.05 and 0.3. The pore volume and size were calculated  
166 from the N<sub>2</sub> desorption values based on the Barrett–Joyner–Halenda (BJH) model [67-69]. The BJH  
167 model determines the mesopore volume distribution, which accounts for the change in adsorbate layer  
168 thickness and the liquid condensed in the pores [70]. The pore volume was calculated as the uptake  
169 (cm<sup>3</sup>/g) at a relative pressure of 0.95.

170

### 171 **2.3.3 Thermogravimetric analysis**

172 Thermogravimetric analysis (TGA) was performed on an SDT Q600 TA instrument (New Castle, DE, USA).  
173 The TGA profiles were used to characterize the thermal stability of MOFs. About 20 mg of sample was  
174 placed in a cylindrical alumina crucible and heated in static air from ambient temperature to 700 °C with

175 a nominal heating rate of 10 °C/min. The change in weight of MOF samples was used to determine the  
176 moisture content, decomposition of the linkers, and formation of metal oxides.

177

#### 178 **2.3.4 Fourier transform infrared spectroscopy**

179 Infrared spectra of the synthesized catalysts were recorded on a JASCO Fourier transform infrared (FTIR)  
180 spectrometer (Easton, MD, USA), equipped with an attenuated total reflection stage (ATR). Samples of  
181 about 5 mg were used in each analysis. The sample was scanned in the spectral range between 400 and  
182 4000  $\text{cm}^{-1}$  at a 4  $\text{cm}^{-1}$  resolution. Spectra were collected using a deuterated triglycine sulfate (DTGS)  
183 detector averaging 256 scans.

184

#### 185 **2.3.5 Diffuse reflectance infrared Fourier transform spectroscopy**

186 Diffuse reflectance infrared Fourier transform spectroscopy (DRIFTS) with adsorbed pyridine was  
187 performed to characterize acid sites; measurements were made with a JASCO FTIR-4700 equipped with  
188 high temperature DiffuseIR™ cell (PIKE Technology, WI, USA). The protocol for the DRIFTS experiments  
189 with temperature programmed desorption is described elsewhere and used with a slight modification  
190 [71, 72]. In short, MOF samples (~5 mg) were placed in a cylindrical alumina crucible and treated in  
191 nitrogen gas (50 mL/min) at 150°C for 30 min unless otherwise noted. After the treatment, the DRIFT  
192 spectra of MOF catalysts were recorded as the background spectra. The MOF catalysts were then  
193 saturated with pyridine vapor in the low of N<sub>2</sub> gas (50 mL/min). The adsorbed pyridine was removed by  
194 flushing with N<sub>2</sub> gas (50 mL/min) at 50, 100, or 150°C for 30 min before recording the DRIFT spectra. All  
195 spectra were recorded with 256 scans between 4000–400  $\text{cm}^{-1}$  at a 4  $\text{cm}^{-1}$  resolution using a mercury  
196 cadmium telluride (MCT) detector cooled with liquid nitrogen. The ratio of Brønsted acid to Lewis acid  
197 sites (B/L) was calculated from the integrated area of the bands (after background subtraction) of  
198 adsorbed pyridine at 1067 and 1030  $\text{cm}^{-1}$  [73].

199 **2.3.6 X-ray diffraction**

200 X-ray diffraction of MOFs was conducted with a Bruker AXS Model D8 Advance A28 diffractometer  
201 (Germany) using  $\text{CuK}\alpha$  radiation in the  $2\theta$  range from  $5^\circ$  to  $40^\circ$  with 0.02 degree/step. Samples of about  
202 200 mg were used in each analysis.

203

204 **2.3.7 Inductively coupled plasma-optical emission spectroscopy**

205 Inductively coupled plasma-optical emission spectroscopy (ICP-OES) measurements were performed  
206 using a 100 mg sample dissolved in 10 mL of nitric acid. Heating was used to ensure that the sample was  
207 completely dissolved. Once cooled, the sample was further diluted to 25 mL with double distilled water.  
208 Measurements were acquired on a Varian 720-ES spectrometer equipped with a seaspray nebulizer and  
209 cyclonic class spray chamber. Parameters included a sample intake of 1 mL/min, argon plasma flow rate  
210 of 15 L/min, and an auxiliary gas (Ar) flow rate of 1.5 L/min. The instrument was calibrated using a CRMS  
211 manufactured by VHG.

212

213 **2.4 Dehydration of glucose**

214 A 50 mg sample of glucose and 1 g  $[\text{C}_4\text{C}_{1\text{im}}]\text{Cl}$  were added to a 25 mL pressure tube. The catalyst was  
215 loaded with respect to the glucose at a glucose:Al molar ratio of 25:1 unless otherwise noted. The  
216 pressure tube was sealed, stirred at 700 RPM (to minimize mass transfer limitations) and kept in an oil  
217 bath at  $120^\circ\text{C}$  unless otherwise noted. The reaction was stopped by quenching in a cold-water bath,  
218 followed by adding water (~5 mL) to dissolve the remaining glucose and prevent the solidification of  
219 ionic liquid. The solution was centrifuged and the residual solids were removed. The liquid sample was  
220 withdrawn and analyzed for changes in glucose and the occurrence of dehydration products.

221 **2.5 Product analysis and quantification**

222 The reactants and products were analyzed by a High-Pressure Liquid Chromatography (HPLC, Agilent  
223 Technology, Santa Clara, CA, USA) equipped with a refractive index detector (RID) and diode array  
224 detector (DAD). An Aminex HPX-87H column (300 x 7.8 mm, Bio-Rad®, Hercules, CA, USA) was used for  
225 reactant and product separation at 60°C with 0.6 mL/min of 4 mM H<sub>2</sub>SO<sub>4</sub> as the mobile phase. The  
226 concentrations of sugars and other products were determined by the peak areas from the RID signals.  
227 The main HMF product was determined by the peak area from the DAD signals at 280 nm. Sugar and  
228 reaction products were calibrated against certified standards (Absolute Standards, Inc., Hamden, CT,  
229 USA). The glucose conversion, product yield, and product selectivity were calculated as follows:

230 
$$\text{Glucose conversion (\%)} = \frac{\text{mole of glucose reacted}}{\text{initial mole of glucose}} \times 100$$

231 
$$\text{Product yield (\%)} = \frac{\text{mole of product generated}}{\text{initial mole of glucose}} \times 100$$

232 
$$\text{Product selectivity (\%)} = \frac{\text{Product yield}}{\text{Glucose conversion}} \times 100$$

233

234 To ensure that the determination of glucose conversion and HMF selectivity were accurate,  
235 control experiments using PTA⊂MIL-101(Al)-NH<sub>2</sub>, ionic liquid, and water were conducted at ambient  
236 temperature for 2h. The change in glucose and HMF concentrations in the presence of MOFs was  
237 negligible (*see Supporting Information and Fig. S1 for detail*). Moreover, to confirm the formation of  
238 HMF, solvent extraction by ethyl acetate was used with the reaction solution. The extracted solution  
239 was analyzed by Agilent gas chromatography-mass spectrometry (GC-MS, model 7890A and 5977A,  
240 Agilent Technologies, Santa Clara, CA, USA) equipped with a DB-1701 column (Agilent Technologies, 30  
241 m × 0.25 mm id, 0.25 μm) (*see Supporting Information and Fig. S2 for detail*).

242

### 243 3. Results

244 Encapsulating phosphotungstic acid (PTA) in MIL-101(Al)-NH<sub>2</sub> (Al-MOF) formed encapsulated PTA@MIL-  
245 101(Al)-NH<sub>2</sub> (PTA@Al-MOF) catalysts. The effect of PTA loading on MOF physicochemical and acid  
246 properties was investigated. Subsequently, the efficiency of PTA@Al-MOF catalysis of glucose  
247 dehydration was measured by comparing the performance of encapsulated PTA catalysts with different  
248 PTA loading.

249

#### 250 3.1 Physicochemical properties of the PTA@MIL-101(Al)-NH<sub>2</sub> catalyst

251 To evaluate the physicochemical properties of the encapsulated PTA@Al-MOF catalysts, first, an N<sub>2</sub>  
252 adsorption-desorption was performed to measure the surface area and pore volume (**Fig. S3A**). The bare  
253 Al-MOF exhibited a Type IV isotherm, which suggested that the MIL-101(Al)-NH<sub>2</sub> catalyst was  
254 mesoporous. On the basis of the isotherms, the MOF total surface area and pore volume were  
255 calculated and shown in **Table 1**. As a control, the surface area and pore volume of Al-MOF were 1487  
256 m<sup>2</sup>/g and 0.92 cc/g, similar to reported values [74, 75]. As expected, an increase in PTA loading  
257 decreased both total surface area and pore volume, which indicated that the encapsulated PTA  
258 occupied the pores of the Al-MOF. The average pore diameter of the synthesized catalysts was ~2.4-2.7  
259 nm, in agreement with reported values of 1.6-2.9 nm [32, 76]. The critical diameter for D-glucose was  
260 ~0.84-0.85 nm [77], which is sufficiently small to enable access to the active sites within the MOF  
261 structure.

262 Next, X-ray diffraction (XRD) was conducted to determine the crystallinity of the encapsulated  
263 PTA@Al-MOF catalysts (**Fig. S3B**). As a control, the X-ray diffractogram of the PTA exhibited unique  
264 peaks at 7.2° and 9.0°, similar to reported values.[78] The consistency between the diffractograms of

265 the encapsulated PTA $\subset$ Al-MOF catalysts and bare Al-MOF suggested that, during synthesis, the PTA $\subset$ Al-  
266 MOF catalysts retained the structural integrity of the MIL-101 framework. These PTA peaks were not  
267 observed in the encapsulated PTA $\subset$ Al-MOF catalysts, which suggested that PTA was well dispersed in  
268 the pores of Al-MOF [78] and/or the PTA clusters in the pentagonal and hexagonal windows of Al-MOF  
269 were indeed smaller than 1.6-1.2 nm [78-80]. Interestingly, the PTA $\subset$ Al-MOF catalysts showed slightly  
270 broader XRD peaks and a shoulder ( $\sim 11^\circ$ ). The peak broadening and occurrence of the shoulder was  
271 hypothesized to be due to the interaction of the encapsulated PTA clusters with the MIL-101 framework,  
272 which resulted in changes in the symmetry of the clusters in the MOF cages. Previous studies using  
273 POM-encapsulated MIL-101 MOFs showed similar XRD peak broadening [29, 30, 52, 55, 81, 82]. To  
274 measure PTA dispersion in the Al-MOF catalyst's pore structure, the encapsulated 14%PTA $\subset$ Al-MOF  
275 catalyst was imaged by STEM-HAADF. As a control, the STEM-HAADF image and elemental mapping of  
276 the bare Al-MOF showed that it was highly porous with dispersed Al (**Figs. 1A and B**). The STEM-HAADF  
277 image and elemental composition mapping of aluminum (Al) and tungsten (W) of the 14%PTA $\subset$ Al-MOF  
278 showed a highly porous and uniform distribution of W and Al clusters within the Al-MOF catalyst (**Figs.**  
279 **1C-F**), which confirmed our XRD data which indicated that PTA was highly dispersed in the pores of the  
280 Al-MOF catalyst.

281 To determine the surface functionality of the synthesized catalysts, FTIR was performed on  
282 catalysts (**Fig. S4**). The bare Al-MOF showed  $-\text{NH}_2$  bands. The FTIR spectra of encapsulated PTA $\subset$ Al-MOF  
283 catalysts contained bands from  $-\text{NH}_2$  and  $\text{W}=\text{O}/\text{W}-\text{O}-\text{W}$  functionalities, which confirmed the  
284 encapsulation of PTA (*see Supplementary Materials, Fig. S4*).

285 During synthesis, the PTA loading was varied from 0.1 to 2.0 g in 30 mL of DMF. To quantify the  
286 actual amount of encapsulated PTA, ICP-OES was conducted on encapsulated PTA $\subset$ Al-MOF catalysts. As  
287 a control, the bare Al-MOF catalyst contained 11.56 wt.% Al, similar to a reported value [30]. All the

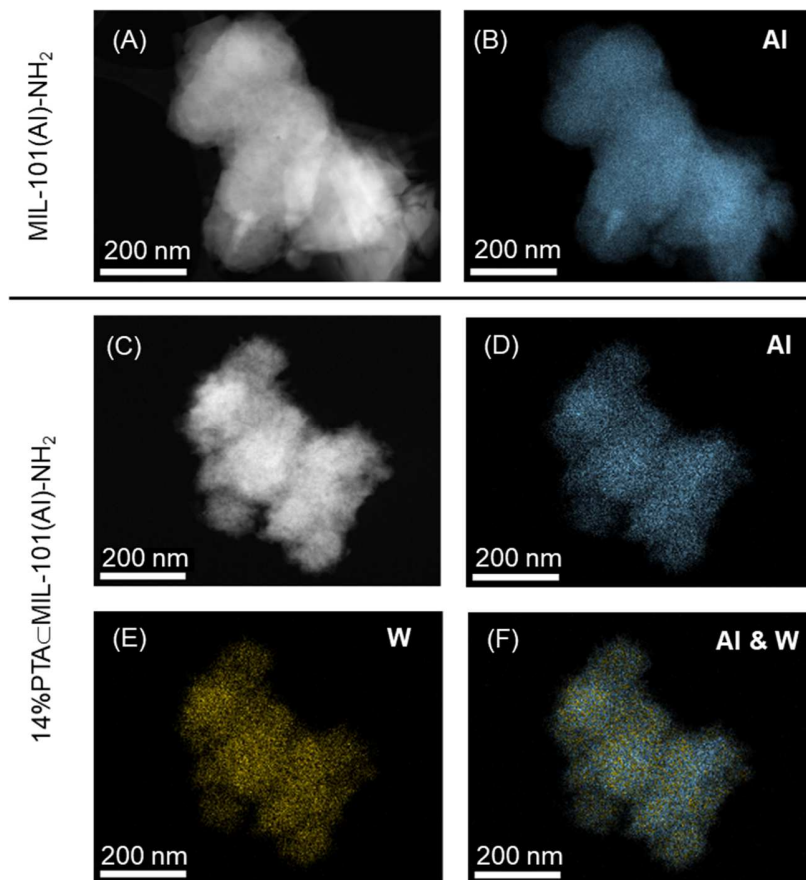
288 encapsulated PTA $\subset$ Al-MOF catalysts had a W/P molar ratio of 12, which was the same as that in PTA  
 289 (H<sub>3</sub>PW<sub>12</sub>O<sub>40</sub>) and which confirmed successful PTA encapsulation [83]. As expected, increases in PTA  
 290 loading during synthesis progressively increased the W content and decreased the Al/W molar ratio.  
 291 Interestingly, a PTA loading greater than 0.25 g/30 mL (entry 3) during synthesis did not result in a  
 292 significant increase in encapsulated PTA. These results suggested that there was an optimal PTA loading  
 293 that could occupy the MOF pores.

**Table 1.** Physicochemical properties of MOFs with varying PTA content

Entry	PTA loading [g/30mL] <sup>a</sup>	Catalyst <sup>b</sup>	Al [wt.%] <sup>c</sup>	W [wt.%] <sup>c</sup>	PTA [wt.%] <sup>c</sup>	Al/W [mol/mol]	B/L <sup>d</sup>	S <sub>BET</sub> [m <sup>2</sup> /g]	Total pore volume [cm <sup>3</sup> /g]	Pore diameter (nm)
1	0.00	NH <sub>2</sub> -MIL-101(Al)	11.56	-	-	-	0.37	1487	0.92	2.49
2	0.10	8%PTA $\subset$ NH <sub>2</sub> -MIL-101(Al)	9.33	6.2	8.1	10.3	0.53	1375	0.82	2.39
3	0.25	14%PTA $\subset$ NH <sub>2</sub> -MIL-101(Al)	9.53	11.03	14.3	5.9	0.78	1276	0.78	2.46
4	0.50	15%PTA $\subset$ NH <sub>2</sub> -MIL-101(Al)	9.19	11.51	15.0	5.4	0.96	1061	0.72	2.72
5	1.00	17%PTA $\subset$ NH <sub>2</sub> -MIL-101(Al)	9.64	13.00	16.9	5.1	1.04	961	0.59	2.45
6	2.00	18%PTA $\subset$ NH <sub>2</sub> -MIL-101(Al)	9.11	13.52	17.5	4.6	1.14	854	0.57	2.69

294 <sup>a</sup>per 30 mL DMF, <sup>b</sup>number before catalyst name indicates the encapsulated PTA measured by ICP-OES, <sup>c</sup>composition measured  
 295 by ICP-OES, <sup>d</sup>B/L indicates Brønsted acid/Lewis acid site ratio from the area integral by diffuse reflectance infrared Fourier  
 296 transform spectroscopy (DRIFTS).

297

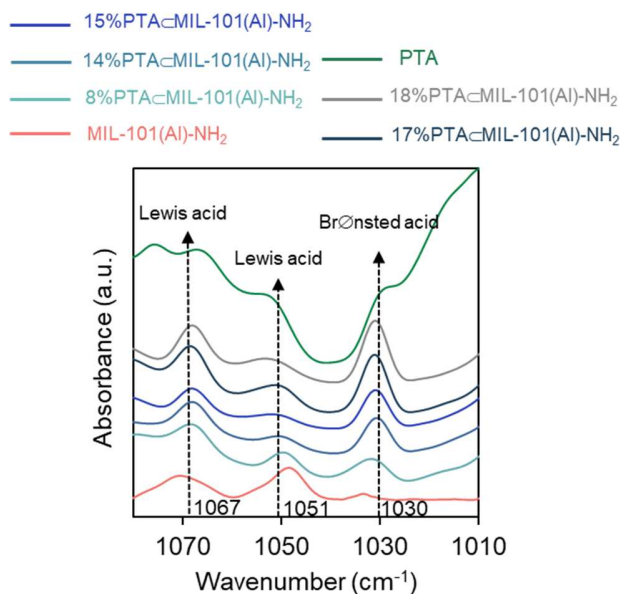


298

299 **Figure 1.** STEM-HAADF images and corresponding elemental mapping of (A-B) MIL-101(AI)-NH<sub>2</sub> and (C-F)

300 14%PTA-MIL-101(AI)-NH<sub>2</sub>.





301

302 **Figure 2.** Acid properties of encapsulated PTA@Al-MOF catalysts measured by diffuse reflectance  
 303 infrared Fourier transform spectroscopy (DRIFTS).

304

### 305 3.2 Acid properties of the catalysts by diffuse reflectance infrared Fourier transform spectroscopy

306 Selective glucose conversion to HMF requires a cooperative effect between Lewis and Brønsted acid  
 307 catalysts for the cascade of glucose isomerization to fructose followed by fructose dehydration to HMF.

308 Hence, it is important to distinguish and quantify the acid sites. To characterize the acid sites of the  
 309 synthesized MOFs, DRIFTS was performed with adsorbed pyridine. Pyridine was chosen as an in-situ  
 310 titrant for probing the acid site density of MOFs because of previous success in observation of Lewis acid  
 311 and Brønsted acid sites in MOFs [84-86]. To avoid degradation of bare Al-MOF and encapsulated  
 312 PTA@Al-MOF catalysts, DRIFTS was performed in a range of 30 - 150°C according to their thermal  
 313 stability from the TGA result (**Fig. S5**). After pyridine adsorption, the DRIFT spectra of these MOFs  
 314 demonstrated characteristic bands at 1067, 1051, and 1030 cm<sup>-1</sup> (**Fig. 2**). The 1067 and 1051 cm<sup>-1</sup> bands

315 corresponded to the interaction between pyridine and coordinated unsaturated metal sites (cus), i.e.,  
316 Lewis acid sites [86, 87]. The band at 1030 cm<sup>-1</sup> corresponded to the interaction between pyridine and  
317 the Brønsted acid sites from encapsulated PTA. Surprisingly, a weak band at 1300 cm<sup>-1</sup> in the MIL-  
318 101(Al)-NH<sub>2</sub> sample was observed, which suggested the presence of Brønsted acidity in MOFs. Similarly,  
319 studies by Herbst et al. [88], Halls et al. [89], Vimont et al. [90], and Volkringer et al. [86] showed that  
320 MIL-101(Cr), MIL-100(Cr), and MIL-100(Al) exhibited Brønsted acidity. The origin of Brønsted acidity in  
321 MOFs remains the topic of debate. However, its origin was hypothesized to come from the water  
322 molecules bound to metal sites [86]. Moreover, this water coordinated to the metal sites was not easily  
323 removed during activation of MOFs because a high temperature was required to remove the bound  
324 water. The high temperature can cause the structural damage to the MOFs and cause a loss in catalytic  
325 activity (*see Supporting Information and Fig. S6 for detail*).

326

327         Next, the Brønsted acid to Lewis acid ratio (B/L) was determined using the area integral of these  
328 bands (**Table 1**). An increase in encapsulated PTA loading increased the intensity of the Brønsted acid  
329 band at 1030 cm<sup>-1</sup> and increased the B/L ratio of the catalysts. It should be noted that an increase in  
330 encapsulated PTA within MOFs was not proportional to an increase in B/L ratio. The acidic properties of  
331 encapsulated catalysts are difficult to be determined because the interaction between encapsulated  
332 species and the host support can modify their acidic properties. Juan-Alcañiz et al. showed the  
333 interaction between encapsulated PTA and the MIL-100(Cr) framework decreased Lewis acidity [91],  
334 which agrees with our finding of an increase in the B/L ratio after encapsulating more PTA because of  
335 an increase in Brønsted acid sites and a decrease in Lewis acid sites.

336

### 337 **3.3 PTA@MIL-101(Al)-NH<sub>2</sub>-catalyzed glucose dehydration to 5-hydroxymethylfurfural**

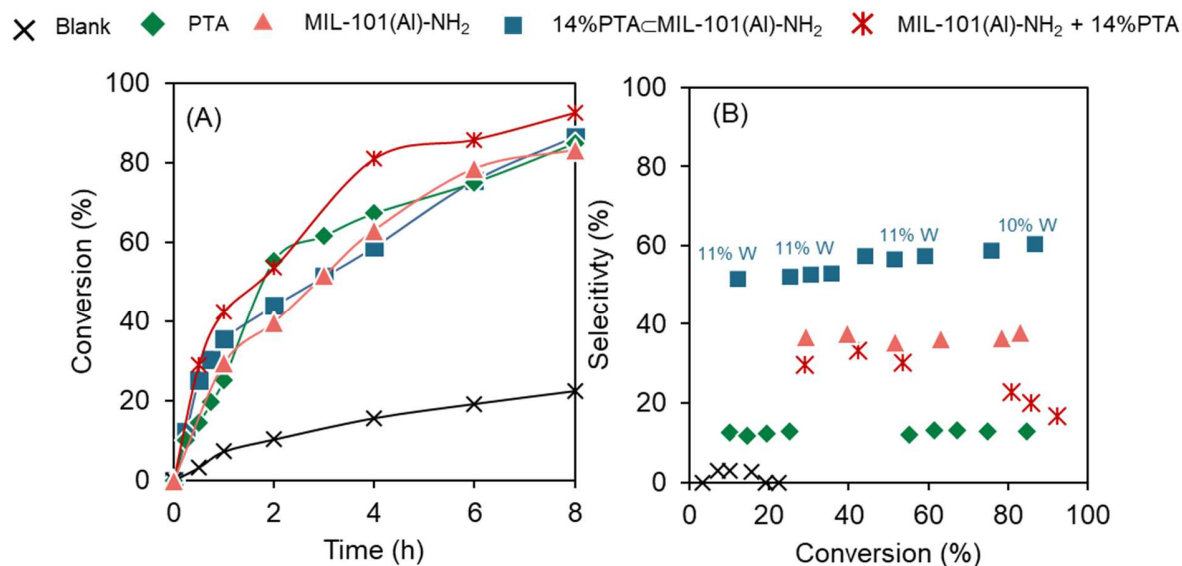
338 To determine the effect of PTA encapsulation on the catalytic performance, glucose dehydration was  
339 performed with encapsulated PTA@MIL-101(Al)-NH<sub>2</sub> catalysts (**Fig. 3**). A glucose:Al molar ratio of 25:1  
340 was used in all experiments to normalize the Al content in the catalysts and compare catalytic  
341 performance with different encapsulated PTA loadings. As a control, a blank (no added catalyst) did not  
342 show any HMF production, which suggested that (1) the reaction is not autocatalytic, and (2) [C<sub>2</sub>C<sub>1</sub>im]Cl  
343 could not catalyze glucose dehydration. All catalysts were active for glucose dehydration in [C<sub>2</sub>C<sub>1</sub>im]Cl at  
344 120°C (**Fig. 3A**). Another control of using PTA as a catalyst showed a low HMF selectivity of 13% at 43%  
345 glucose conversion. Fructose, levulinic acid, or formic acid were not observed as products. These results  
346 suggested the PTA catalyst was not selective to HMF as in previous studies [52]. The bare Al-MOF  
347 catalyst appeared to be an efficient catalyst for glucose dehydration; however, it was not the most  
348 selective for HMF. All encapsulated PTA@Al-MOF catalysts were more selective for HMF than MIL-  
349 101(Al)-NH<sub>2</sub>, which indicated that the encapsulated PTA in the pores of the Al-MOF enhanced HMF  
350 selectivity (**Fig. S7**). Moreover, HMF selectivity exhibited a volcano-shaped profile vs. the Brønsted to  
351 Lewis acid site ratio (B/L) (**Fig. 4**). The optimal B/L of 0.78 (14%PTA@Al-MOF catalyst) maximized the  
352 HMF selectivity of 58% at 44% glucose conversion at 120°C after 2h (**Fig. 3B**). These results suggested  
353 that cooperativity between Brønsted acidic PTA and Lewis acid sites of Al-MOF catalyst enhanced HMF  
354 selectivity.

355 To determine the importance of encapsulating PTA, a glucose dehydration reaction was  
356 performed with a physical mix of PTA and bare Al-MOF catalyst at the same composition as 14%PTA@Al-  
357 MOF catalyst. HMF selectivity by the physical mix catalyst was 33%, lower than that of encapsulated  
358 14%PTA@Al-MOF catalysts (58%). These results confirmed the importance of PTA encapsulation in  
359 maximizing HMF selectivity. Interestingly, the HMF selectivity of the physically mixed catalyst converged  
360 to that of PTA alone (**Fig. 3B**). Although the Brønsted acid such as PTA catalyzes fructose dehydration to  
361 HMF, the free PTA molecules in the physical mix can catalyze aldol addition and condensation reactions

362 from HMF via 2,5-dioxo-6-hydroxyhexanal [92], which resulted in humin formation. Moreover, the free  
 363 PTA in the physical mix has a strong interaction with the surface of MOF, partially blocking the channels  
 364 of MOFs and inhibiting the reactant accessibility to active sites [93, 94]. This blocking effect is the reason  
 365 why the HMF selectivity of the physical mix was lower than that of encapsulated PTA in MOFs [78]. Thus,  
 366 the physical mix showed a high glucose conversion with a poor HMF selectivity, in agreement with the  
 367 study by Zhang et al. [52].

368 To evaluate the stability of PTA in encapsulated PTA@MIL-101(Al)-NH<sub>2</sub> catalysts during the  
 369 reaction, ICP-OES was performed on spent encapsulated 14%PTA@MIL-101(Al)-NH<sub>2</sub> catalyst (**Fig. 3B**).  
 370 The W content of the encapsulated 14%PTA@MIL-101(Al)-NH<sub>2</sub> catalyst remained relatively constant (~11  
 371 wt.% W), which confirmed the stability of the PTA within the 14%PTA@MIL-101(Al)-NH<sub>2</sub> catalyst.

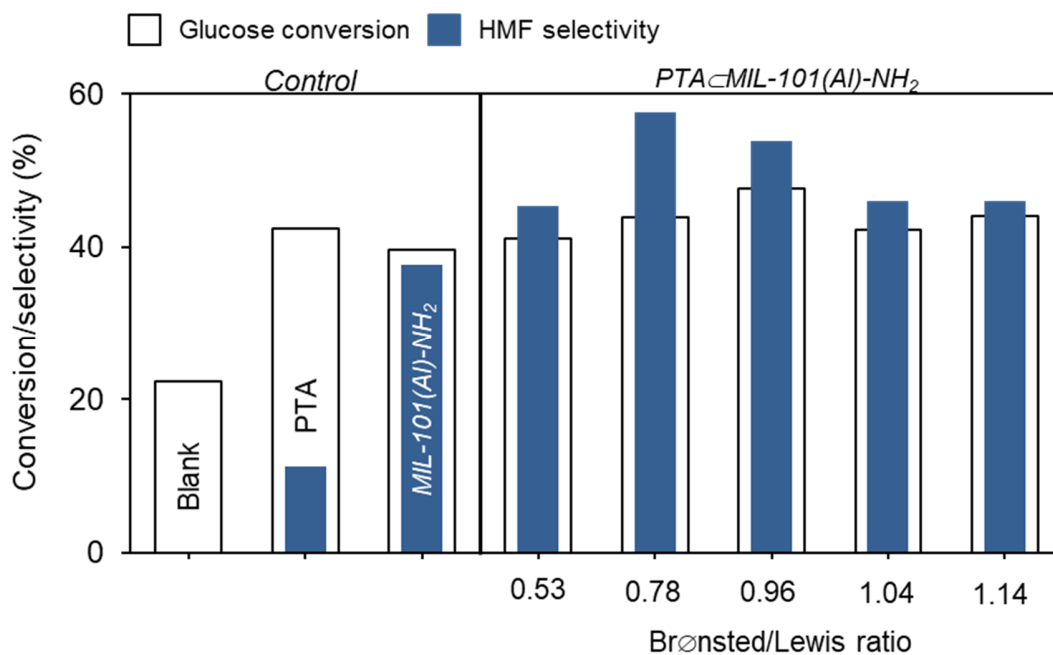
372



373

374 **Figure 3.** Catalytic performance of encapsulated PTA@MIL-101(Al)-NH<sub>2</sub> catalysts. (A) Catalyst activity for  
 375 glucose dehydration as a function of time. (B) HMF selectivity with the W content of the spent catalysts

376 assessed by ICP-OES. Reaction condition: glucose:Al molar ratio=25:1, 50 mg glucose, 1 g [C<sub>4</sub>C<sub>1</sub>im]Cl,  
 377 120°C. Phosphotungstic acid = 14 wt.% in PTA alone and physical mix between PTA + bare Al-MOF to  
 378 match the PTA in 14%PTA⊂Al-MOF. The percent of tungsten (%W) in **Figure 3B** indicates the W content  
 379 in the used catalyst at the specific conversion.



380  
 381 **Figure 4.** HMF selectivity of encapsulated PTA⊂MIL-101(Al)-NH<sub>2</sub> catalysts at similar glucose conversions.  
 382 Reaction condition: glucose:Al molar ratio=25:1, 50 mg glucose, 1 g [C<sub>4</sub>C<sub>1</sub>im]Cl, 120°C, 2h.

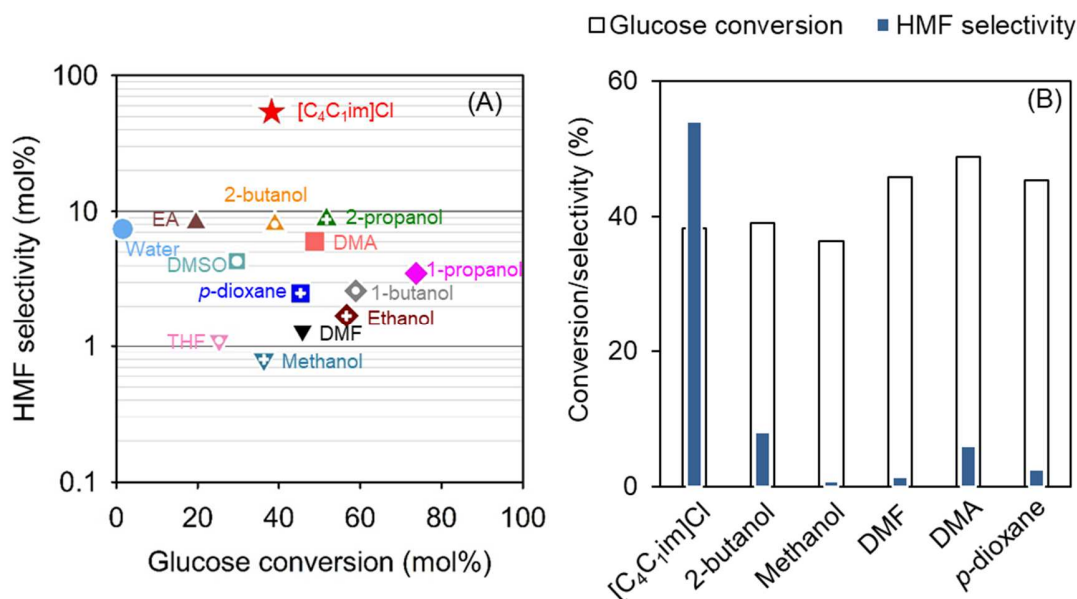
383  
 384 **3.4 Solvent effect on the glucose dehydration to 5-hydroxymethylfurfural**

385 The solvent affects the rate of reaction, product selectivity, and product stability [95, 96]. A major  
 386 consideration in catalytic biomass conversion is the stability of reactants, intermediates, and product in  
 387 the reaction solvent. To investigate the effect of solvent on the stability of these molecules, glucose,  
 388 fructose and HMF were used as reactants in various solvents. The 14%PTA⊂Al-MOF was chosen as

389 catalyst because it had the greatest HMF selectivity. For glucose, [C<sub>4</sub>C<sub>1</sub>im]Cl was the best performing  
390 solvent as shown by the greatest HMF selectivity at similar conversion to other solvents (**Fig. 5**).  
391 However, there was no obvious correlation between the HMF selectivity and solvent properties, such as  
392 dielectric constant or donor number.

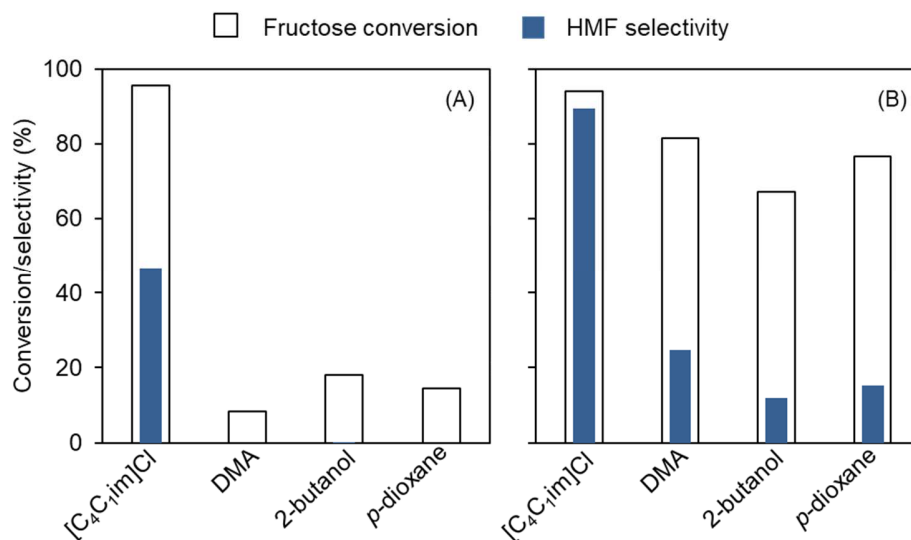
393           Next, fructose was used as a reactant in [C<sub>4</sub>C<sub>1</sub>im]Cl (**Fig. 6**). Three solvents, DMA, 2-butanol, and  
394 *p*-dioxane, were selected for comparison with [C<sub>4</sub>C<sub>1</sub>im]Cl. Without added catalyst (blank), HMF  
395 selectivity was 47% at 96% fructose conversion in [C<sub>4</sub>C<sub>1</sub>im]Cl. The other solvents did not yield HMF and  
396 showed <20% fructose conversion. As expected, added 14%PTA◊MIL-101(Al)-NH<sub>2</sub> catalyst improved the  
397 HMF selectivity in all solvents; more specifically, HMF selectivity in [C<sub>4</sub>C<sub>1</sub>im]Cl was 89% at 94% fructose  
398 conversion, two times greater HMF selectivity compared with a reaction without added catalyst.  
399 Although added 14%PTA◊MIL-101(Al)-NH<sub>2</sub> catalyst improved the fructose conversion in DMA, 2-  
400 butanol, and *p*-dioxane from <20% to >60%, the HMF selectivity in these three solvents was low (<22%).  
401 These results suggested that [C<sub>4</sub>C<sub>1</sub>im]Cl can act as both acid catalyst [97, 98] and solvent in fructose  
402 dehydration reaction. Moreover, the 14%PTA◊MIL-101(Al)-NH<sub>2</sub> enhanced HMF selectivity from fructose  
403 dehydration.

404



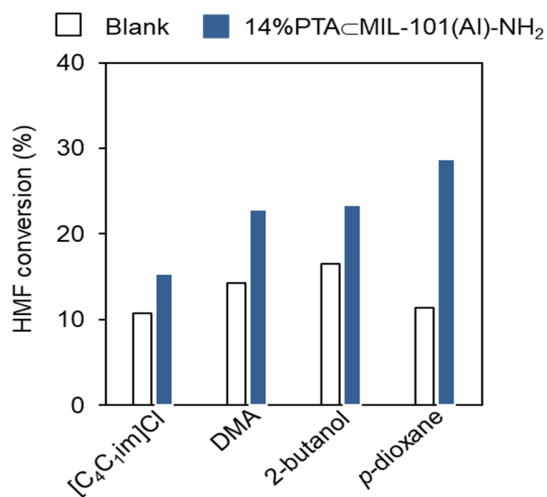
405  
 406 **Figure 5.** Solvent effect on glucose conversion and HMF selectivity (A) and comparison of conversion and  
 407 selectivity in selected solvents(B) by using 14%PTA◊MIL-101(Al)-NH<sub>2</sub> catalyst. Reaction condition:  
 408 glucose:Al molar ratio=25:1, 50 mg glucose, 1 g solvent, 120°C, 2 h.

409  
 410 Next, HMF was used as a reactant in these four solvents to investigate the HMF stability (**Fig. 7**).  
 411 Without any catalyst(blank), HMF conversion was 11% in [C<sub>4</sub>C<sub>1</sub>im]Cl, and conversion increased slightly in  
 412 other solvents. There were no identifiable products which suggests the HMF was likely degraded into  
 413 humin [99, 100]. The added 14%PTA◊MIL-101(Al)-NH<sub>2</sub> catalyst enhanced HMF conversion to 15% in  
 414 [C<sub>4</sub>C<sub>1</sub>im]Cl. The presence of 14%PTA◊MIL-101(Al)-NH<sub>2</sub> catalyst in other solvents improved the HMF  
 415 conversion more than in [C<sub>4</sub>C<sub>1</sub>im]Cl. These results suggested that (1) HMF was not stable in these  
 416 solvents and (2) although the 14%PTA◊MIL-101(Al)-NH<sub>2</sub> catalyst improved glucose/fructose dehydration  
 417 to HMF, the catalyst facilitated HMF conversion to humin. Thus, to minimize HMF degradation and  
 418 maintain the high HMF yield, a reactive HMF extraction process should be considered [101].



419

420 **Figure 6.** Solvent effect on fructose conversion to HMF (A) without added catalyst and (B) catalytic  
 421 performance of encapsulated 14%PTA-MIL-101(Al)-NH<sub>2</sub>. Reaction condition: fructose:Al molar ratio =  
 422 25:1, 50 mg fructose, 1 g solvent, 120°C, 2h.



423

424 **Figure 7.** HMF conversion in different solvents with/without 14%PTA-MIL-101(Al)-NH<sub>2</sub>. Reaction  
 425 condition: HMF:Al molar ratio = 25:1, 50 mg HMF, 1 g solvent, 120°C, 2h.

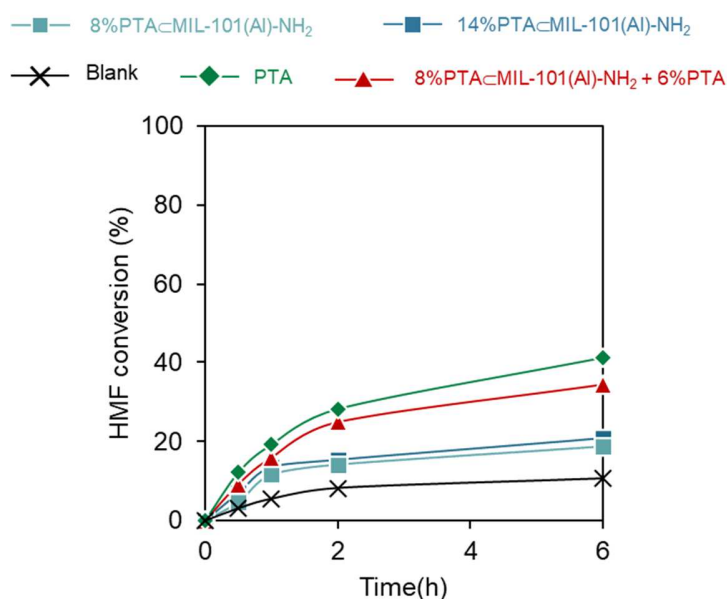
426



### 427 3.5 Stability of HMF in the catalytic system and [C<sub>4</sub>C<sub>1</sub>im]Cl

428 To maintain the high HMF selectivity in the reaction, it was important to determine the stability of the  
429 HMF under the reaction condition. Thus, HMF was heated in the same experimental condition that was  
430 used for glucose dehydration (120°C) in [C<sub>4</sub>C<sub>1</sub>im]Cl solvent and catalysts. Without catalysts (blank), HMF  
431 degradation was ~11% after 6h (**Fig. 8**). Levulinic acid and formic acid were not observed. These results  
432 suggested that [C<sub>4</sub>C<sub>1</sub>im]Cl was not able to rehydrate HMF. With added encapsulated 8% and  
433 14%PTA⊂Al-MOF catalysts, a slight increase in HMF conversion was observed, which reached ~18% after  
434 6h. With PTA alone, the HMF conversion rate was 41%, greater than that of conversion in the presence  
435 of encapsulated 8% and 14%PTA⊂Al-MOF catalysts and reaching 19% and 21% after 6h, respectively.

436 Next, the physical mixture of PTA and 8%PTA⊂MIL-101(Al)-NH<sub>2</sub> catalyst was evaluated to check  
437 the HMF stability. The amount of PTA in the physical mixture of PTA and 8%PTA⊂Al-MOF catalyst was  
438 maintained at the same level as for the encapsulated 14%PTA⊂Al-MOF catalyst. As expected, the  
439 physical mixture increased HMF conversion by 34% at 6h reaction time compared with 21% HMF  
440 conversion by 14%PTA⊂Al-MOF catalyst. These results demonstrated that PTA in the bulk solution  
441 degraded the HMF and decreased the HMF selectivity, similar to a finding of Zhang et al. [52]. The  
442 encapsulation of PTA in the pores of Al-MOF catalyst minimized PTA leaching into the solvent and  
443 limited conversion of HMF, which, in turn, maintained the HMF selectivity.



444

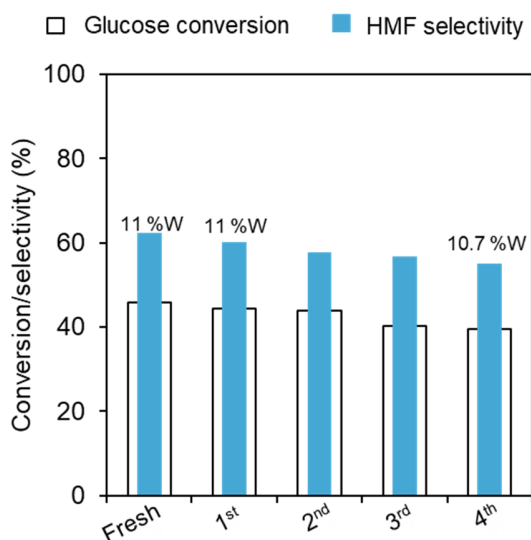
445 **Figure 8.** HMF conversion by encapsulated PTA@MIL-101(AI)-NH<sub>2</sub>. Reaction condition: 50 mg HMF, 30  
 446 mg catalyst, 1 g solvent, 120°C. Phosphotungstic acid = 14 wt.% in PTA alone and physical mix between  
 447 6%PTA + 8%Al-MOF to match the PTA in 14%PTA@Al-MOF.

448

### 449 3.6 Reuse of encapsulated PTA@MIL-101(AI)-NH<sub>2</sub> for glucose dehydration

450 To determine the ability to reuse the encapsulated PTA@Al-MOF catalyst, the used catalyst was  
 451 recovered by centrifugation, washed with water, and dried in a vacuum oven at 130°C to remove  
 452 moisture, residual products, intermediates, and unreacted glucose. Then, the catalyst was reused four  
 453 times. The 14%PTA@Al-MOF was chosen because it had the greatest HMF selectivity. The 14%PTA@Al-  
 454 MOF catalyst maintained its catalytic performance with HMF selectivity of ~ 55% at 40% glucose  
 455 conversion after the 4<sup>th</sup> cycle, <10% decrease in both glucose conversion and HMF selectivity compared  
 456 with fresh catalyst (**Fig. 9**). In all cycles, the selectivity to HMF was between 55-62%. Next, ICP-EOS was  
 457 used to measure the Tungsten(W) content in the used catalysts. Only a slight W loss (<3 wt.%) in the

458 used catalysts was observed after four recycles, which indicated that little to no PTA leached from the  
459 14%PTA $\subset$ Al-MOF catalyst.



460

461 **Figure 9.** Reuse of 14%PTA $\subset$ MIL-101(Al)-NH<sub>2</sub> for glucose dehydration. Reaction condition: glucose: Al  
462 molar ratio = 25:1, 1 g [C<sub>4</sub>C<sub>1</sub>im]Cl, 120°C, 2 h. Tungsten content (%W) indicates the W content in the  
463 used catalyst.

464

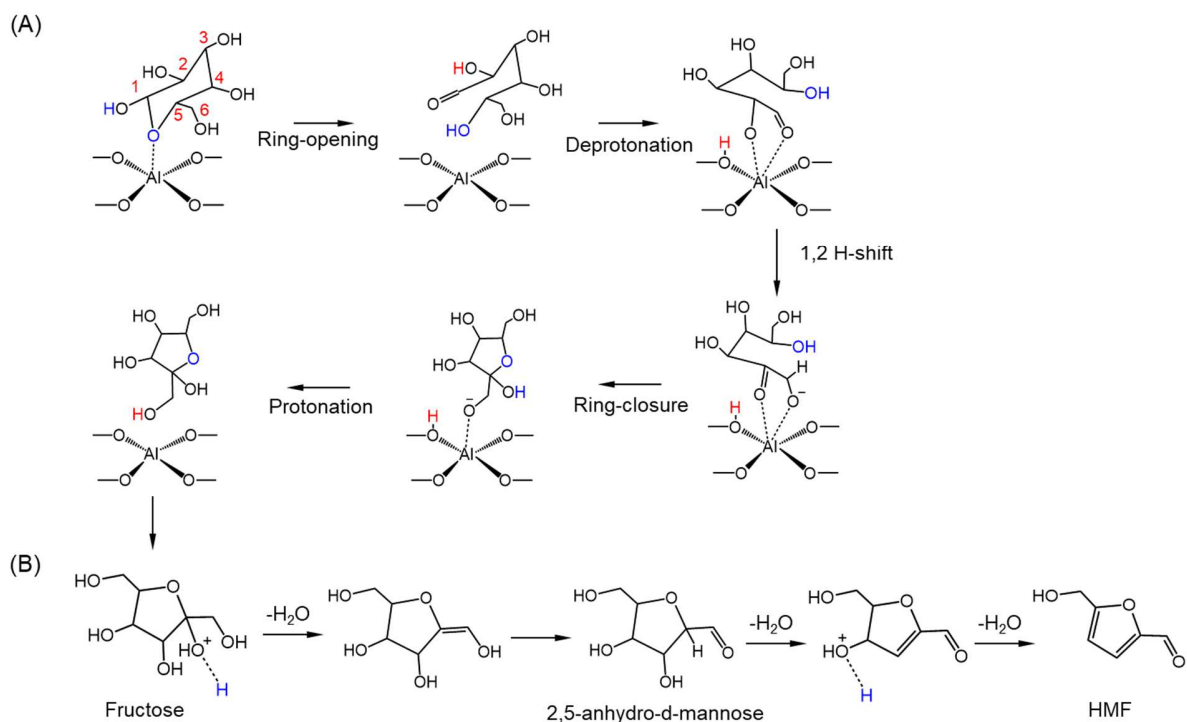
### 465 3.7 Proposed chemical pathway for glucose dehydration to HMF by PTA $\subset$ MIL-101(Al)-NH<sub>2</sub>

466 On the basis of the foregoing findings, **Scheme 2** shows a proposed mechanism for glucose dehydration  
467 to HMF by PTA $\subset$ MIL-101(Al)-NH<sub>2</sub> catalysts. The reaction proceeds by the synergy between Lewis-Brønsted  
468 acid sites: (1) glucose isomerization to fructose by the Lewis acid of MIL-101(Al)-NH<sub>2</sub>, and (2) dehydration  
469 of resulting fructose to HMF by the Brønsted acid of PTA and/or MIL-101(Al)-NH<sub>2</sub>.

470 The glucose isomerization to fructose by Lewis acid sites consists of a sequence of ring opening,  
471 deprotonation, isomerization, protonation, and ring closure processes as shown by Hensen et al. [102-  
472 104]. We postulated that glucose initially binds to the Al active site imbedded in the MIL-101 framework

473 via its ring oxygen atom and followed by the ring opening process to form the acyclic glucose.  
 474 Subsequently, the deprotonation of the hydroxyl group at C<sub>2</sub> occurred by the metal-oxo clusters. Next,  
 475 the aldose-ketose isomerization induces the hydride shift from the C<sub>2</sub> to C<sub>1</sub> carbon atom. The reaction  
 476 undergoes a ring-closure reaction yielding anionic fructofuranose bound to Al site. Finally, the terminal  
 477 oxygen anionic fructofuranose is protonated to generate fructose.

478 The fructose undergoes dehydration by Brønsted acid sites to produce HMF by dehydration and  
 479 tautomerization. First, the hydroxyl group of the fructose at the alpha position is protonated by acidic  
 480 protons of Brønsted acid catalysts, which resulted in the formation of water. Next, the cyclic enol  
 481 intermediate is formed and subsequently tautomerized to 2,5-anhydro-d-mannose [105-107]. Then, the  
 482 reaction proceeds by two sequential dehydrations to form HMF.



483

484 **Scheme 2.** Proposed reaction mechanism for glucose dehydration to HMF over PTA@MIL-101(Al)-NH<sub>2</sub>.  
485 The reaction proceeds by (A) glucose dehydration to fructose, followed by (B) fructose dehydration to  
486 HMF.

487

#### 488 **4. Discussion**

489 A major challenge in selective glucose conversion to HMF is the design of catalysts that possess Lewis  
490 and Brønsted acid sites that can act cooperatively [15, 108, 109]. Here, the effect of PTA encapsulation  
491 in PTA@MIL-101(Al)-NH<sub>2</sub> catalysts (PTA@Al-MOF) on glucose conversion to HMF was investigated. The  
492 synergy between encapsulated PTA and Al-MOFs enabled the high HMF selectivity. Moreover, the  
493 results demonstrated that the encapsulation of PTA in MIL-101(Al)-NH<sub>2</sub> catalysts minimized PTA leaching  
494 into the bulk solution, thereby preventing degradation of the HMF product.

495 The most significant finding was that the HMF selectivity strongly depended on the location of  
496 the PTA. Encapsulation of PTA in MIL-101(Al)-NH<sub>2</sub> pores provided two benefits. First, the close proximity  
497 between the Lewis acid sites of the Al-MOF and the Brønsted acidic PTA promoted HMF formation. The  
498 fructose formed from glucose isomerization by Lewis acid (MIL-101(Al)-NH<sub>2</sub>) was dehydrated to HMF by  
499 the encapsulated PTA catalyst. Tangsermit et al. showed that the proximity between Lewis and  
500 Brønsted acid sites was important in achieving a high HMF yield [110], a result that agrees with our  
501 findings. Second, encapsulated PTA catalysts minimized PTA leaching into the bulk solution and,  
502 consequently, prevented HMF degradation. Although Brønsted acids catalyze fructose dehydration to  
503 HMF, they also catalyze undesired HMF rehydration to levulinic acid [111] and/or degradation to humin  
504 [11]. The MIL-101 structure of the Al-MOF possesses both mesoporous windows (29-34 Å) and  
505 microporous windows, the latter corresponding to large hexagonal pores (15-16 Å), and somewhat  
506 smaller pentagonal pores (~12 Å) [112-114]. Keggin-type heteropolyacids, ~13-14 Å in size [53], are

507 larger than the pentagonal pores in MIL-101, thereby the heteropolyacids are preventing from leaching  
508 out and causing side reactions (rehydration and/or humin formation). These results explained the  
509 retention of HMF selectivity and the ability to recycle the PTA⊂MIL-101(Al)-NH<sub>2</sub> catalyst. Hence,  
510 encapsulated Brønsted acidic PTA in the pores of MIL-101(Al)-NH<sub>2</sub> not only provided Brønsted acidity for  
511 fructose dehydration but also prevented PTA leaching into the bulk solution, that otherwise had the  
512 potential to degrade HMF.

513 Another significant finding was the discovery of the high selectivity of PTA⊂Al-MOF for glucose  
514 dehydration. Many investigators used solid Lewis acid catalysts (Sn-containing β-zeolites [20] and Nb<sub>2</sub>O<sub>5</sub>  
515 [18]) with homogeneous catalysts such as HCl to maximize HMF selectivity (**Table S3**). Their results  
516 suggested that the cooperative effect between Lewis acid and Brønsted acid species was critical in  
517 maximizing HMF selectivity in glucose dehydration. Qu et al. impregnated SO<sub>4</sub><sup>2-</sup> on ZrO<sub>2</sub> by H<sub>2</sub>SO<sub>4</sub> acid  
518 [115]. Although the SO<sub>4</sub><sup>2-</sup>/ZrO<sub>2</sub> in biphasic THF/H<sub>2</sub>O system reached a high HMF selectivity of 67% at 93%  
519 glucose conversion, both HMF selectivity and glucose conversion dropped ~10% after the 4<sup>th</sup> catalyst  
520 recycling due to leaching of SO<sub>4</sub><sup>2-</sup> [115]. The ability to create the solid bifunctional Lewis-Brønsted  
521 catalysts will enhance the commercial feasibility of HMF production. Zhang et al. encapsulated PTA in  
522 MIL-101(Cr) to produce the bifunctional acid catalysts with PTA as a Brønsted acid and MIL-101(Cr) as a  
523 Lewis acid [52]. The PTA⊂MIL-101(Cr) catalysts were selective toward HMF in fructose dehydration.  
524 However, they were not selective toward HMF in glucose dehydration and gave only 10% HMF  
525 selectivity at 21% glucose conversion at 100°C after 3h. Compared with MOF-derived catalysts for  
526 glucose dehydration, the PTA⊂Al-MOF catalysts described in this report were superior to other MOF-  
527 derived catalysts in terms of HMF selectivity (**Table S3**).

528 These findings demonstrate that PTA⊂Al-MOF catalyst was a selective and recyclable catalyst  
529 for glucose dehydration to HMF. The PTA⊂MIL-101(Al)-NH<sub>2</sub> catalyst was easy to synthesize compared

530 with other solid acid catalysts for selective glucose conversion to HMF, such as modified  $\beta$ -zeolites [116].  
531 Moreover, the ability to control the ratio of numbers of Brønsted acid sites to Lewis acid sites in PTA $\subset$ Al-  
532 MOF catalysts provides opportunities to use the catalysts in various organic reactions, such as  
533 esterification [117], alkylation [118], and benzylation [119].

534 Although PTA $\subset$ Al-MOF catalyst is promising for selective glucose conversion to HMF, the  
535 interactions between the framework, metal nodes, and PTA (acidic protons) that affect the acid  
536 properties and catalytic performance has not been extensively investigated. Juan-Alcañiz et al. reported  
537 the partial W substitution by Cr<sup>3+</sup> of MIL-101(Cr) at high temperatures [53]. The W-substituted  
538 heteropolyacids and/or the formation of W-Al complex metal nodes might be the active sites for this  
539 reaction. Additional studies should identify the interaction between W in PTA and Al in Al-MOF by <sup>27</sup>Al  
540 Magic Angle Spin (MAS) Nuclear Magnetic Resonance (NMR). The knowledge will help in designing  
541 selective catalysts and systems for glucose dehydration.

542

## 543 **5. Conclusion**

544 Phosphotungstic acid encapsulated MIL-101(Al)-NH<sub>2</sub> catalyst (PTA $\subset$ MIL-101(Al)-NH<sub>2</sub>) was developed for  
545 selective glucose conversion to HMF. The encapsulation of Brønsted acidic phosphotungstic acid in the  
546 pores of MIL-101(Al)-NH<sub>2</sub> provided the proximity between Brønsted acid sites and Lewis acid sites of  
547 MIL-101(Al)-NH<sub>2</sub> for the efficient cascade of glucose isomerization and fructose dehydration. The  
548 synergistic effect of Brønsted and Lewis acid sites in the phosphotungstic acid encapsulated MIL-101(Al)-  
549 NH<sub>2</sub> catalyst is the key contributor to the high HMF selectivity and glucose conversion; this synergy  
550 cannot occur if the agents are introduced separately. Moreover, the encapsulated phosphotungstic acid  
551 was stable in the pores of MIL-101(Al)-NH<sub>2</sub>, which minimized leaching of PTA into the bulk solution and  
552 reaction with the HMF to generate undesired products. As a result, the encapsulated PTA $\subset$ MIL-101(Al)-

553 NH<sub>2</sub> catalyst maintained its catalytic performance after recycling four times. These results underscore  
554 the importance of phosphotungstic acid encapsulation to provide the cooperative effect between  
555 Brønsted and Lewis acidic sites for maximizing the HMF formation and minimizing subsequent HMF  
556 conversion/degradation. This encapsulated metal-organic framework catalyst should be applicable to  
557 other acid-catalyzed biomass transformations.

558

### 559 **Acknowledgment**

560 A part of this material is based upon work supported by the National Science Foundation under  
561 Cooperative Agreement No. 1355438 and Internal Research Grant, Office of the Executive Vice President  
562 for Research, University of Louisville. This work was performed in part at the Conn Center for Renewable  
563 Energy Research at the University of Louisville, which belongs to the National Science Foundation NNCI  
564 KY Manufacturing and Nano Integration Node, supported by ECCS-1542174. The authors would like to  
565 thank Dr. Howard Fried for his valuable comments and suggestions on the manuscript.

566

### 567 **References**

- 568 [1] Regnier E. Oil and energy price volatility. *Energy Econ* 2007;29(3):405-27.  
569 [2] Awodumi OB, Adewuyi AO. The role of non-renewable energy consumption in economic growth  
570 and carbon emission: Evidence from oil producing economies in Africa. *Energy Strategy Rev*  
571 2020;27:100434.  
572 [3] Kuster BFM. 5-Hydroxymethylfurfural (HMF). A review focussing on its manufacture. *Starch-*  
573 *Stärke* 1990;42(8):314-21.  
574 [4] Fan C, Guan H, Zhang H, Wang J, Wang S, Wang X. Conversion of fructose and glucose into 5-  
575 hydroxymethylfurfural catalyzed by a solid heteropolyacid salt. *Biomass and bioenergy*  
576 2011;35(7):2659-65.  
577 [5] Yong G, Zhang Y, Ying JY. Efficient catalytic system for the selective production of 5-  
578 hydroxymethylfurfural from glucose and fructose. *Angew Chem Int Ed* 2008;47(48):9345-8.  
579 [6] Xu H, Wang Z, Huang J, Jiang Y. Thermal Catalytic Conversion of Biomass-Derived Glucose to Fine  
580 Chemicals. *Energy Fuels* 2021;35:8602-16.  
581 [7] Wrigstedt P, Keskiaväli J, Leskelä M, Repo T. The Role of Salts and Brønsted Acids in Lewis Acid-  
582 Catalyzed Aqueous-Phase Glucose Dehydration to 5-Hydroxymethylfurfural. *ChemCatChem*  
583 2015;7(3):501-7.



- 584 [8] Yang L, Tsilomelekis G, Caratzoulas S, Vlachos DG. Mechanism of Brønsted Acid-Catalyzed  
585 Glucose Dehydration. *ChemSusChem* 2015;8(8):1334-41.
- 586 [9] van Putten RJ, Soetedjo J, Pidko E, van der Waal J, Hensen E, de Jong E, et al. Dehydration of  
587 different ketoses and aldoses to 5-hydroxymethylfurfural. *ChemSusChem* 2013;6(9):1681-7.
- 588 [10] Ordonsky V, Sushkevich V, Schouten J, Van Der Schaaf J, Nijhuis T. Glucose dehydration to 5-  
589 hydroxymethylfurfural over phosphate catalysts. *J Catal* 2013;300:37-46.
- 590 [11] Shen J, Wyman CE. Hydrochloric acid-catalyzed levulinic acid formation from cellulose: data and  
591 kinetic model to maximize yields. *AIChE J* 2012;58(1):236-46.
- 592 [12] Caratzoulas S, Davis M, Gorte R, Gounder R, Lobo R, Nikolakis V, et al. Challenges of and insights  
593 into acid-catalyzed transformations of sugars. *J Phys Chem C* 2014;118(40):22815-33.
- 594 [13] Kruger JS, Nikolakis V, Vlachos DG. Aqueous-phase fructose dehydration using Brønsted acid  
595 zeolites: Catalytic activity of dissolved aluminosilicate species. *Appl Catal, A* 2014;469:116-23.
- 596 [14] Román-Leshkov Y, Moliner M, Labinger JA, Davis ME. Mechanism of glucose isomerization using  
597 a solid Lewis acid catalyst in water. *Angew Chem Int Ed* 2010;49(47):8954-7.
- 598 [15] Pagan-Torres YJ, Wang T, Gallo JMR, Shanks BH, Dumesic JA. Production of 5-  
599 hydroxymethylfurfural from glucose using a combination of Lewis and Brønsted acid catalysts in  
600 water in a biphasic reactor with an alkylphenol solvent. *ACS Catal* 2012;2(6):930-4.
- 601 [16] Chen SS, Maneerung T, Tsang DCW, Ok YS, Wang CH. Valorization of biomass to  
602 hydroxymethylfurfural, levulinic acid, and fatty acid methyl ester by heterogeneous catalysts.  
603 *Chem Eng J* 2017;328:246-73.
- 604 [17] Bounoukta CE, Megías-Sayago C, Ammari F, Ivanova S, Monzon A, Centeno MA, et al.  
605 Dehydration of glucose to 5-hydroxymethylfurfural on bifunctional carbon catalysts. *Appl Catal,*  
606 *B* 2021;286:119938.
- 607 [18] Vieira JL, Almeida-Trapp M, Mithöfer A, Plass W, Gallo JMR. Rationalizing the conversion of  
608 glucose and xylose catalyzed by a combination of Lewis and Brønsted acids. *Catal Today*  
609 2020;344:92-101.
- 610 [19] Swift TD, Nguyen H, Anderko A, Nikolakis V, Vlachos DG. Tandem Lewis/Brønsted homogeneous  
611 acid catalysis: conversion of glucose to 5-hydroxymethylfurfural in an aqueous chromium (III)  
612 chloride and hydrochloric acid solution. *Green Chem* 2015;17(10):4725-35.
- 613 [20] Nikolla E, Román-Leshkov Y, Moliner M, Davis M. "One-pot" synthesis of 5-(hydroxymethyl)  
614 furfural from carbohydrates using tin-beta zeolite. *ACS Catal* 2011;1(4):408-10.
- 615 [21] Cole-Hamilton DJ. Homogeneous catalysis--new approaches to catalyst separation, recovery,  
616 and recycling. *Science* 2003;299(5613):1702-6.
- 617 [22] Farrusseng D, Aguado S, Pinel C. Metal-organic frameworks: opportunities for catalysis. *Angew*  
618 *Chem Int Ed* 2009;48(41):7502-13.
- 619 [23] Lee J, Farha OK, Roberts J, Scheidt KA, Nguyen ST, Hupp JT. Metal-organic framework materials  
620 as catalysts. *Chem Soc Rev* 2009;38(5):1450-9.
- 621 [24] Férey G. Hybrid porous solids: past, present, future. *Chem Soc Rev* 2008;37(1):191-214.
- 622 [25] Li H, Eddaoudi M, O'Keeffe M, Yaghi OM. Design and synthesis of an exceptionally stable and  
623 highly porous metal-organic framework. *Nature* 1999;402(6759):276-9.
- 624 [26] Kitagawa S, Kitaura R, Noro S-I. Functional porous coordination polymers. *Angew Chem Int Ed*  
625 2004;43(18):2334-75.
- 626 [27] Dhakshinamoorthy A, Alvaro M, Garcia H. Commercial metal-organic frameworks as  
627 heterogeneous catalysts. *Chem Commun* 2012;48(92):11275-88.
- 628 [28] Chen Y, Zhou Y, Wang H, Lu J, Uchida T, Xu Q, et al. Multifunctional PdAg@ MIL-101 for one-pot  
629 cascade reactions: combination of host-guest cooperation and bimetallic synergy in catalysis.  
630 *ACS Catal* 2015;5(4):2062-9.

- 631 [29] Henschel A, Gedrich K, Kraehnert R, Kaskel S. Catalytic properties of MIL-101. *Chem Commun* 2008(35):4192-4.  
632
- 633 [30] Bromberg L, Su X, Hatton TA. Heteropolyacid-functionalized aluminum 2-aminoterephthalate  
634 metal-organic frameworks as reactive aldehyde sorbents and catalysts. *ACS Appl Mater*  
635 *Interfaces* 2013;5(12):5468-77.
- 636 [31] Toyao T, Fujiwaki M, Horiuchi Y, Matsuoka M. Application of an amino-functionalised metal-  
637 organic framework: An approach to a one-pot acid-base reaction. *Rsc Adv* 2013;3(44):21582-7.
- 638 [32] Serra-Crespo P, Ramos-Fernandez EV, Gascon J, Kapteijn F. Synthesis and characterization of an  
639 amino functionalized MIL-101 (Al): separation and catalytic properties. *Chem Mater*  
640 2011;23(10):2565-72.
- 641 [33] Srirambalaji R, Hong S, Natarajan R, Yoon M, Hota R, Kim Y, et al. Tandem catalysis with a  
642 bifunctional site-isolated Lewis acid-Brønsted base metal-organic framework, NH<sub>2</sub>-MIL-101(Al).  
643 *Chem Commun* 2012;48(95):11650-2.
- 644 [34] Ramos-Fernandez EV, Pieters C, van der Linden B, Juan-Alcañiz J, Serra-Crespo P, Verhoeven M,  
645 et al. Highly dispersed platinum in metal organic framework NH<sub>2</sub>-MIL-101 (Al) containing  
646 phosphotungstic acid-Characterization and catalytic performance. *J Catal* 2012;289:42-52.
- 647 [35] Ma L, Abney C, Lin W. Enantioselective catalysis with homochiral metal-organic frameworks.  
648 *Chem Soc Rev* 2009;38(5):1248-56.
- 649 [36] Corma A, García H, Llabrés i Xamena FX. Engineering metal organic frameworks for  
650 heterogeneous catalysis. *Chem Rev* 2010;110(8):4606-55.
- 651 [37] Yoon M, Srirambalaji R, Kim K. Homochiral metal-organic frameworks for asymmetric  
652 heterogeneous catalysis. *Chem Rev* 2012;112(2):1196-231.
- 653 [38] Jiang J, Yaghi OM. Brønsted acidity in metal-organic frameworks. *Chem Rev* 2015;115(14):6966-  
654 97.
- 655 [39] Horn MR, Singh A, Alomari S, Goberna-Ferrón S, Benages-Vilau R, Chodankar N, et al.  
656 Polyoxometalates (POMs): from electroactive clusters to energy materials. *Energy Environ Sci*  
657 2021;14(4):1652-700.
- 658 [40] Gumerova NI, Rompel A. Synthesis, structures and applications of electron-rich  
659 polyoxometalates. *Nat Rev Chem* 2018;2(2):0112.
- 660 [41] Kazanskij LP, Spitsyn VI. Proton-acceptor capacity and energy of oxygen 1s-electrons of  
661 heteropolyanions. *Dokl Akad Nauk SSSR* 1976;227(1):140-3.
- 662 [42] Misono M. Recent progress in the practical applications of heteropolyacid and perovskite  
663 catalysts: Catalytic technology for the sustainable society. *Catal Today* 2009;144(3-4):285-91.
- 664 [43] Wang SS, Yang GY. Recent advances in polyoxometalate-catalyzed reactions. *Chem Rev*  
665 2015;115(11):4893-962.
- 666 [44] Deng W, Zhang Q, Wang Y. Polyoxometalates as efficient catalysts for transformations of  
667 cellulose into platform chemicals. *Dalton Trans* 2012;41(33):9817-31.
- 668 [45] Weinstock IA, Schreiber RE, Neumann R. Dioxygen in polyoxometalate mediated reactions.  
669 *Chem Rev* 2017;118(5):2680-717.
- 670 [46] Enferadi-Kerenkan A, Do TO, Kaliaguine S. Heterogeneous catalysis by tungsten-based  
671 heteropoly compounds. *Catal Sci Technol* 2018;8(9):2257-84.
- 672 [47] Zhong J, Perez-Ramirez J, Yan N. Biomass valorisation over polyoxometalate-based catalysts.  
673 *Green Chem* 2021;23:18-36.
- 674 [48] Wang C, Zhang L, Zhou T, Chen J, Xu F. Synergy of Lewis and Brønsted acids on catalytic  
675 hydrothermal decomposition of carbohydrates and corncob acid hydrolysis residues to 5-  
676 hydroxymethylfurfural. *Sci Rep* 2017;7:40908.
- 677 [49] Wang Z, Chen Q. Conversion of 5-hydroxymethylfurfural into 5-ethoxymethylfurfural and ethyl  
678 levulinate catalyzed by MOF-based heteropolyacid materials. *Green Chem* 2016;18(21):5884-9.

- 679 [50] Zhan G, Zeng HC. Integrated nanocatalysts with mesoporous silica/silicate and microporous  
680 MOF materials. *Coord Chem Rev* 2016;320:181-92.
- 681 [51] Liang DD, Liu SX, Ma FJ, Wei F, Chen YG. A crystalline catalyst based on a porous metal-organic  
682 framework and 12-tungstosilicic acid: Particle size control by hydrothermal synthesis for the  
683 formation of dimethyl ether. *Adv Synth Catal* 2011;353(5):733-42.
- 684 [52] Zhang Y, Degirmenci V, Li C, Hensen EJM. Phosphotungstic acid encapsulated in metal-organic  
685 framework as catalysts for carbohydrate dehydration to 5-hydroxymethylfurfural.  
686 *ChemSusChem* 2011;4(1):59-64.
- 687 [53] J, Ramos-Fernandez EV, Lafont U, Gascon J, Kapteijn F. Building MOF bottles around  
688 phosphotungstic acid ships: One-pot synthesis of bi-functional polyoxometalate-MIL-101  
689 catalysts. *J Catal* 2010;269(1):229-41.
- 690 [54] Sun M. A PTA@MIL-101(Cr)-diatomite composite as catalyst for efficient oxidative  
691 desulfurization. *Inorg Chem Commun* 2018;87:30-5.
- 692 [55] Maksimchuk NV, Kovalenko KA, Arzumanov SS, Chesalov YA, Melgunov MS, Stepanov AG, et al.  
693 Hybrid polyoxotungstate/MIL-101 materials: synthesis, characterization, and catalysis of H<sub>2</sub>O<sub>2</sub>-  
694 based alkene epoxidation. *Inorg Chem* 2010;49(6):2920-30.
- 695 [56] Su Y, Chang G, Zhang Z, Xing H, Su B, Yang Q, et al. Catalytic dehydration of glucose to 5-  
696 hydroxymethylfurfural with a bifunctional metal-organic framework. *AIChE J* 2016;62(12):4403-  
697 17.
- 698 [57] Das AP, Mishra S. Hexavalent chromium (VI): Environment pollutant and health hazard. *J Environ*  
699 *Res Dev* 2008;2(3):386-92.
- 700 [58] Tulaphol S, Hossain MA, Rahaman MS, Liu LY, Phung TK, Rennecker S, et al. Direct production of  
701 levulinic acid in one pot from hemp hurd by dilute acid in ionic liquids. *Energy Fuels*  
702 2019;32(2):1764-72.
- 703 [59] Sun N, Liu H, Sathitsuksanoh N, Stavila V, Sawant M, Bonito A, et al. Production and extraction of  
704 sugars from switchgrass hydrolyzed in ionic liquids. *Biotechnol Biofuels* 2013;6(1):1-15.
- 705 [60] Groff D, George A, Sun N, Sathitsuksanoh N, Bokinsky G, Simmons BA, et al. Acid enhanced ionic  
706 liquid pretreatment of biomass. *Green Chem* 2013;15(5):1264-7.
- 707 [61] Kozhevnikov IV. Advances in catalysis by heteropolyacids. *Russ Chem Rev* 1987;56(9):811.
- 708 [62] Bromberg L. Heteropolyacid-functionalized aluminum 2-aminoterephthalate metal-organic  
709 frameworks as reactive aldehyde sorbents and catalysts. *ACS Appl Mater Interfaces*  
710 2013;5(12):5468-77.
- 711 [63] Haul R. SJ Gregg, KSW Sing: adsorption, surface area and porosity. 2. auflage, academic press,  
712 London 1982. 303 Seiten, Preis: \$49.50. Wiley Online Library; 1982.
- 713 [64] Sing KSW. Reporting physisorption data for gas/solid systems with special reference to the  
714 determination of surface area and porosity (Recommendations 1984). *Pure Appl Chem*  
715 1985;57(4):603-19.
- 716 [65] Jaroniec M, Kruk M, Sayari A. Adsorption methods for characterization of surface and structural  
717 properties of mesoporous molecular sieves. *Stud. Surf. Sci. Catal.: Elsevier*; 1998, p. 325-32.
- 718 [66] Dollimore D, Spooner P, Turner A. The BET method of analysis of gas adsorption data and its  
719 relevance to the calculation of surface areas. *Surf Technol* 1976;4(2):121-60.
- 720 [67] Barrett EP, Joyner LG, Halenda PP. The determination of pore volume and area distributions in  
721 porous substances. I. Computations from nitrogen isotherms. *J Am Chem Soc* 1951;73(1):373-  
722 80.
- 723 [68] Xu J, Liu J, Li Z, Wang X, Wang Z. Synthesis, structure and properties of Pd@ MOF-808. *J Mater*  
724 *Sci* 2019;54(19):12911-24.

- 725 [69] Jana SK, Nishida R, Shindo K, Kugita T, Namba S. Pore size control of mesoporous molecular  
726 sieves using different organic auxiliary chemicals. *Microporous Mesoporous Mater* 2004;68(1-  
727 3):133-42.
- 728 [70] Groen JC, Peffer LAA, Pérez-Ramírez J. Pore size determination in modified micro-and  
729 mesoporous materials. Pitfalls and limitations in gas adsorption data analysis. *Microporous*  
730 *Mesoporous Mater* 2003;60(1-3):1-17.
- 731 [71] Osman AI, Abu-Dahrieh JK, Rooney DW, Halawy SA, Mohamed MA, Abdelkader A. Effect of  
732 precursor on the performance of alumina for the dehydration of methanol to dimethyl ether.  
733 *Appl Catal, B* 2012;127:307-15.
- 734 [72] Santos KM, Albuquerque EM, Innocenti G, Borges LE, Sievers C, Fraga MA. The role of Brønsted  
735 and water-tolerant Lewis acid sites in the cascade aqueous-phase reaction of triose to lactic  
736 acid. *ChemCatChem* 2019.
- 737 [73] Yu D, Wu M, Hu Q, Wang L, Lv C, Zhang L. Iron-based metal-organic frameworks as novel  
738 platforms for catalytic ozonation of organic pollutant: Efficiency and mechanism. *J Hazard Mater*  
739 2019;367:456-64.
- 740 [74] Li SW, Wang W, Zhao JS. Effective and reusable oxidative desulfurization of dibenzothiophene  
741 via magnetic amino-MIL-101 supported  $H_3PMo_6W_6O_{40}$  components: comparison influence on  
742 various types of MIL-101. *Energy Fuels* 2020;34(4):4837-48.
- 743 [75] Qin L, Li Z, Hu Q, Xu Z, Guo X, Zhang G. One-pot assembly of metal/organic-acid sites on amine-  
744 functionalized ligands of MOFs for photocatalytic hydrogen peroxide splitting. *Chem Commun*  
745 2016;52(44):7110-3.
- 746 [76] Wang J, Liu Y, Guo X, Qu H, Chang R, Ma J. Efficient Adsorption of Dyes Using Polyethyleneimine-  
747 Modified NH<sub>2</sub>-MIL-101 (Al) and its Sustainable Application as a Flame Retardant for an Epoxy  
748 Resin. *ACS omega* 2020;5(50):32286-94.
- 749 [77] Jae J, Tompsett GA, Foster AJ, Hammond KD, Auerbach SM, Lobo RF, et al. Investigation into the  
750 shape selectivity of zeolite catalysts for biomass conversion. *J Catal* 2011;279(2):257-68.
- 751 [78] Lin ZJ, Zheng HQ, Chen J, Zhuang WE, Lin YX, Su JW, et al. Encapsulation of phosphotungstic acid  
752 into metal-organic frameworks with tunable window sizes: Screening of PTA@MOF catalysts for  
753 efficient oxidative desulfurization. *Inorg Chem* 2018;57(20):13009-19.
- 754 [79] Bromberg L, Diao Y, Wu H, Speakman SA, Hatton TA. Chromium(III) Terephthalate Metal Organic  
755 Framework (MIL-101): HF-Free Synthesis, Structure, Polyoxometalate Composites, and Catalytic  
756 Properties. *Chem Mater* 2012;24(9):1664-75.
- 757 [80] Navarro-Sánchez J, Almora-Barrios N, Lerma-Berlanga B, Ruiz-Pernía JJ, Lorenz-Fonfria VA,  
758 Tuñón I, et al. Translocation of enzymes into a mesoporous MOF for enhanced catalytic activity  
759 under extreme conditions. *Chem Sci* 2019;10(14):4082-8.
- 760 [81] Maksimchuk NV, Timofeeva MN, Melgunov MS, Shmakov AN, Chesalov YA, Dybtsev DN, et al.  
761 Heterogeneous selective oxidation catalysts based on coordination polymer MIL-101 and  
762 transition metal-substituted polyoxometalates. *J Catal* 2008;257(2):315-23.
- 763 [82] Sun C, Liu S, Liang D, Shao K, Ren Y, Su Z. Highly stable crystalline catalysts based on a  
764 microporous metal-organic framework and polyoxometalates. *J Am Chem Soc*  
765 2009;131(5):1883-8.
- 766 [83] Li X, Guo W, Gao X, Yue X. Phosphotungstic acid encapsulated in MIL-53(Fe) as efficient visible-  
767 light photocatalyst for rhodamine B degradation. *Environ Prog Sustainable Energy*  
768 2017;36(5):1342-50.
- 769 [84] Hall JN, Bollini P. Metal-organic framework MIL-100 catalyzed acetalization of benzaldehyde  
770 with methanol: Lewis or Brønsted acid catalysis? *ACS Catal* 2020;10(6):3750-63.

- 771 [85] Zheng XX, Fang ZP, Dai ZJ, Cai JM, Shen LJ, Zhang YF, et al. Iron-based metal–organic frameworks  
772 as platform for H<sub>2</sub>S selective conversion: Structure-dependent desulfurization activity. *Inorg*  
773 *Chem* 2020;59(7):4483-92.
- 774 [86] Volkringer C, Leclerc H, Lavalley JC, Loiseau T, Ferey G, Daturi M, et al. Infrared spectroscopy  
775 investigation of the acid sites in the metal–organic framework aluminum trimesate MIL-100 (Al).  
776 *J Phys Chem C* 2012;116(9):5710-9.
- 777 [87] Leclerc H, Vimont A, Lavalley JC, Daturi M, Wiersum AD, Llewellyn PL, et al. Infrared study of the  
778 influence of reducible iron (III) metal sites on the adsorption of CO, CO<sub>2</sub>, propane, propene and  
779 propyne in the mesoporous metal–organic framework MIL-100. *Phys Chem Chem Phys*  
780 2011;13(24):11748-56.
- 781 [88] Herbst A, Khutia A, Janiak C. Brønsted instead of Lewis acidity in functionalized MIL-101Cr MOFs  
782 for efficient heterogeneous (nano-MOF) catalysis in the condensation reaction of aldehydes  
783 with alcohols. *Inorg Chem* 2014;53(14):7319-33.
- 784 [89] Hall J, Bollini P. Metal–Organic Framework MIL-100 Catalyzed Acetalization of Benzaldehyde  
785 with Methanol: Lewis or Brønsted Acid Catalysis? *ACS Catal* 2020;10(6):3750-63.
- 786 [90] Vimont A, Goupil J-M, Lavalley J-C, Daturi M, Surblé S, Serre C, et al. Investigation of acid sites in  
787 a zeotypic giant pores chromium (III) carboxylate. *J Am Chem Soc* 2006;128(10):3218-27.
- 788 [91] Juan-Alcañiz J, Goesten M, Ramos-Fernandez E, Gascon J, Kapteijn F. Towards efficient  
789 polyoxometalate encapsulation in MIL-100 (Cr): Influence of synthesis conditions. *New J Chem*  
790 2012;36(4):977-87.
- 791 [92] Patil S, Lund C. Formation and growth of humins via aldol addition and condensation during  
792 acid-catalyzed conversion of 5-hydroxymethylfurfural. *Energy Fuels* 2011;25(10):4745-55.
- 793 [93] Maksimchuk N, Kholdeeva O, Kovalenko K, Fedin V. MIL-101 Supported Polyoxometalates:  
794 Synthesis, Characterization, and Catalytic Applications in Selective Liquid-Phase Oxidation. *Isr J*  
795 *Chem* 2011;51(2):281-9.
- 796 [94] Song J, Luo Z, Britt D, Furukawa H, Yaghi O, Hardcastle K, et al. A multiunit catalyst with  
797 synergistic stability and reactivity: a polyoxometalate–metal organic framework for aerobic  
798 decontamination. *J Am Chem Soc* 2011;133(42):16839-46.
- 799 [95] Hou Q, Li W, Zhen M, Liu L, Chen Y, Yang Q, et al. An ionic liquid–organic solvent biphasic system  
800 for efficient production of 5-hydroxymethylfurfural from carbohydrates at high concentrations.  
801 *RSC Adv* 2017;7(75):47288-96.
- 802 [96] Zhao P, Cui H, Zhang Y, Zhang Y, Wang Y, Zhang Y, et al. Synergetic Effect of Brønsted/Lewis Acid  
803 Sites and Water on the Catalytic Dehydration of Glucose to 5-Hydroxymethylfurfural by  
804 Heteropolyacid-Based Ionic Hybrids. *ChemistryOpen* 2018;7(10):824-32.
- 805 [97] Li H, Yang S. Catalytic Transformation of Fructose and Sucrose to HMF with Proline-Derived Ionic  
806 Liquids under Mild Conditions. *Int J Chem Eng* 2014;2014:978708.
- 807 [98] Kumar K, Dahiya A, Patra T, Upadhyayula S. Upgrading of HMF and Biomass-Derived Acids into  
808 HMF Esters Using Bifunctional Ionic Liquid Catalysts under Solvent Free Conditions.  
809 *ChemistrySelect* 2018;3(22):6242-8.
- 810 [99] Xu Z, Yang Y, Yan P, Xia Z, Liu X, Zhang ZC. Mechanistic understanding of humin formation in the  
811 conversion of glucose and fructose to 5-hydroxymethylfurfural in [BMIM]Cl ionic liquid. *RSC Adv*  
812 2020;10(57):34732-7.
- 813 [100] Tsilomelekis G, Orella MJ, Lin Z, Cheng Z, Zheng W, Nikolakis V, et al. Molecular structure,  
814 morphology and growth mechanisms and rates of 5-hydroxymethyl furfural (HMF) derived  
815 humins. *Green Chem* 2016;18(7):1983-93.
- 816 [101] Hou Q, Qi X, Zhen M, Qian H, Nie Y, Bai C, et al. Biorefinery roadmap based on catalytic  
817 production and upgrading 5-hydroxymethylfurfural. *Green Chem* 2021;23(1):119-231.

- 818 [102] Pidko E, Degirmenci V, van Santen R, Hensen E. Glucose activation by transient Cr<sup>2+</sup> dimers.  
819 *Angew Chem Int Ed* 2010;122(14):2584-8.
- 820 [103] Pidko E, Degirmenci V, Hensen E. On the mechanism of Lewis acid catalyzed glucose  
821 transformations in ionic liquids. *ChemCatChem* 2012;4(9):1263-71.
- 822 [104] Yang G, Pidko E, Hensen E. The mechanism of glucose isomerization to fructose over Sn-BEA  
823 zeolite: a periodic density functional theory study. *ChemSusChem* 2013;6(9):1688-96.
- 824 [105] Tangsermvit V, Pila T, Boekfa B, Somjit V, Klysubun W, Limtrakul J, et al. Incorporation of Al<sup>3+</sup>  
825 Sites on Brønsted Acid Metal–Organic Frameworks for Glucose-to-Hydroxymethylfurfural  
826 Transformation. *Small* 2021;17(22):2006541.
- 827 [106] Newth F. The formation of furan compounds from hexoses. *Adv Carbohydr Chem* 1951;6:83-106.
- 828 [107] Antal Jr M, Mok W, Richards G. Mechanism of formation of 5-(hydroxymethyl)-2-furaldehyde  
829 from D-fructose and sucrose. *Carbohydr Res* 1990;199(1):91-109.
- 830 [108] Teong SP, Yi G, Zhang Y. Hydroxymethylfurfural production from bioresources: past, present and  
831 future. *Green Chem* 2014;16(4):2015-26.
- 832 [109] Li X, Peng K, Liu X, Xia Q, Wang Y. Comprehensive Understanding of the Role of Brønsted and  
833 Lewis Acid Sites in Glucose Conversion into 5-Hydroxymethylfurfural. *ChemCatChem*  
834 2017;9(14):2739-46.
- 835 [110] Tangsermvit V, Pila T, Boekfa B, Somjit V, Klysubun W, Limtrakul J, et al. Incorporation of Al<sup>3+</sup>  
836 sites on Brønsted acid metal–organic frameworks for glucose-to-hydroxymethylfurfural  
837 transformation. *Small* 2021:2006541.
- 838 [111] Choudhary V, Mushrif SH, Ho C, Anderko A, Nikolakis V, Marinkovic NS, et al. Insights into the  
839 interplay of Lewis and Brønsted acid catalysts in glucose and fructose conversion to 5-  
840 (hydroxymethyl) furfural and levulinic acid in aqueous media. *JACS* 2013;135(10):3997-4006.
- 841 [112] Férey G, Mellot-Draznieks C, Serre C, Millange F, Dutour J, Surblé S, et al. A chromium  
842 terephthalate-based solid with unusually large pore volumes and surface area. *Science*  
843 2005;309(5743):2040-2.
- 844 [113] Luo QX, Song XD, Ji M, Park SE, Hao C, Li YQ. Molecular size- and shape-selective Knoevenagel  
845 condensation over microporous Cu<sub>3</sub>(BTC)<sub>2</sub> immobilized amino-functionalized basic ionic liquid  
846 catalyst. *Appl Catal, A* 2014;478:81-90.
- 847 [114] Hwang YK, Hong DY, Chang JS, Jung SH, Seo YK, Kim J, et al. Amine grafting on coordinatively  
848 unsaturated metal centers of MOFs: consequences for catalysis and metal encapsulation. *Angew*  
849 *Chem Int Ed* 2008;120(47):4144-8.
- 850 [115] Qu Y, Zhao Y, Xiong S, Wang C, Wang S, Zhu L, et al. Conversion of Glucose into 5-  
851 Hydroxymethylfurfural and Levulinic Acid Catalyzed by SO<sub>4</sub><sup>2-</sup>/ZrO<sub>2</sub> in a Biphasic Solvent  
852 System. *Energy Fuels* 2020;34(9):11041-9.
- 853 [116] Dijkmans J, Gabriëls D, Dusselier M, de Clippel F, Vanelderden P, Houthoofd K, et al. Productive  
854 sugar isomerization with highly active Sn in dealuminated β zeolites. *Green Chem*  
855 2013;15(10):2777-85.
- 856 [117] Tao M, Xue L, Sun Z, Wang S, Wang X, Shi J. Tailoring the synergistic Brønsted-Lewis acidic  
857 effects in heteropolyacid catalysts: Applied in esterification and transesterification reactions. *Sci*  
858 *Rep* 2015;5(1):13764.
- 859 [118] Liu N, Pu X, Wang X, Shi L. Study of alkylation on a Lewis and Brønsted acid hybrid catalyst and  
860 its industrial test. *J Ind Eng Chem* 2014;20(5):2848-57.
- 861 [119] Li B, Leng K, Zhang Y, Dynes JJ, Wang J, Hu Y, et al. Metal–organic framework based upon the  
862 synergy of a Brønsted acid framework and Lewis acid centers as a highly efficient heterogeneous  
863 catalyst for fixed-bed reactions. *J Am Chem Soc* 2015;137(12):4243-8.

864

